Atmos. Chem. Phys. Discuss., 8, 13689–13739, 2008
www.atmos-chem-phys-discuss.net/8/13689/2008/

Atmospheric Chemistry and Physics Discussions

Measurements of OH and HO_2 concentrations during the MCMA-2006 field campaign – Part 1: Deployment of the Indiana University laser-induced fluorescence instrument

S. Dusanter[1], D. Vimal[1,*], P. S. Stevens[1], R. Volkamer[2,3,4], and L. T. Molina[2,5]

[1]Center for Research in Environmental Science, School of Public and Environmental Affairs, Dept. of Chemistry, Indiana Univ., Bloomington, USA
[2]Massachusetts Institute of Technology, Cambridge MA, USA
[3]University of California at San Diego, La Jolla CA, USA
[4]University of Colorado at Boulder and CIRES, Boulder, CO, USA
[5]Molina Center for Energy and the Environment, La Jolla CA, USA
[*]now at: Molecular Physics Laboratory, SRI International, Menlo Park, CA, USA

Received: 5 June 2008 – Accepted: 9 June 2008 – Published: 17 July 2008

Correspondence to: S. Dusanter (sdusante@indiana.edu)

Published by Copernicus Publications on behalf of the European Geosciences Union.

Abstract

Measurements of tropospheric hydroxyl (OH) and hydroperoxy (HO_2) radicals were made during the MCMA (Mexico City Metropolitan Area) field campaign as part of the MILAGRO (Megacity Initiative: Local and Global Research Observations) project during March 2006. These radicals were measured using a laser-induced fluorescence instrument developed at Indiana University. This new instrument takes advantage of the Fluorescence Assay by Gas Expansion technique (FAGE) together with direct excitation and detection of OH at 308 nm. HO_2 is indirectly measured as OH by titration with NO inside the fluorescence cell. At this stage of development, IU-FAGE is capable of detecting 3.9×10^5 molec cm^{-3} of both OH and HO_2, with a signal to noise ratio of 1, an averaged laser power of 10 mW and an averaging time of 5 min. The calibration accuracies (1σ) are ±17% for OH and ±18% for HO_2 using the water-vapor photolysis/O_2 actinometry calibration technique.

OH and HO_2 concentrations were successfully measured at an urban site in Mexico City, with observed concentrations comparable to those measured in other polluted environments. Enhanced levels of OH and HO_2 radicals were observed on several days between 09:30–11 a.m. and suggest an intense photochemistry during morning hours that may be due to elevated sources of HO_x ($OH+HO_2$) and a fast cycling between the radicals under the high NO_x conditions of the MCMA. A comparison with other urban and sub-urban field measurements suggests that OH concentrations are highly buffered under these conditions. In contrast, HO_2 concentrations are highly variable between different urban sites.

1 Introduction

Hydroxyl (OH) and hydroperoxy (HO_2) radicals have been a subject of considerable interest since it was suggested that OH was produced at sufficient concentrations in the troposphere to initiate the oxidation of volatile organic compounds (VOCs) and other

ACPD

8, 13689–13739, 2008

trace gases (Levy, 1971, 1972). Such processes lead to the production of organic peroxy radicals (RO_2), which are converted back into OH via HO_2 through successive reactions involving nitric oxide (NO). Because of its high reactivity, OH controls lifetime and fate of most ambient trace gases and therefore is an important oxidant in the gas-phase photochemistry of the troposphere.

Urban environments are typically characterized by high concentrations of nitrogen oxides (NO_x=NO+NO_2) and VOCs. These areas exhibit a complex oxidation chemistry involving odd hydrogen radicals (HO_x=OH+HO_2), VOCs, and NO_x that leads to the formation of ozone and secondary aerosols. Understanding the coupling between HO_x and NO_x in the presence of VOCs is essential for the design of efficient strategies seeking to reduce the impact of anthropogenic emissions on air quality over urbanized areas. Measurements of OH and HO_2 can provide a critical test of our understanding of this fast photochemistry (Heard and Pilling, 2003).

Laser-induced fluorescence is a versatile technique for the sensitive detection of simple molecules such as OH, as well as HCHO and NO_2, both in the laboratory and in the free atmosphere (Clemitshaw, 2004). This technique has been used successfully to measure HO_x radicals in the stratosphere (Wennberg et al., 1995) and in the troposphere (Heard and Pilling, 2003) using two different excitation-detection schemes. Initial instruments were based on OH excitation at 282 nm and red-shifted fluorescence detection at 308 nm, allowing optical filtering of the OH fluorescence from the intense scattered laser-light. This detection scheme has been applied with success in the stratosphere, but is not applicable in the troposphere where the higher ambient pressure and the high content of water-vapor lead to the production of OH from the photodissociation of O_3 at 282 nm (R1) by the laser beam, and the subsequent reaction of the photo-product, $O(^1D)$, with water-vapor:

$$O_3 + h\nu \rightarrow O(^1D) + O_2 \quad \text{(R1)}$$

$$O(^1D) + H_2O \rightarrow OH + OH \quad \text{(R2)}$$

The laser-generated OH can be detected within the same laser pulse that produced it,

ACPD
8, 13689–13739, 2008

resulting in a quadratic dependence of the detected OH signal with laser power.

In order to reduce the O_3-water photolytic interference, while keeping a high instrumental sensitivity, a second detection technique based on OH excitation and detection at 308 nm and at low-pressure is widely used for tropospheric measurements (Heard and Pilling, 2003). Ambient air is expanded inside a detection cell and OH is probed by low-energy laser-pulses generated at a high repetition-rate. This sampling technique, known as Fluorescence Assay by Gas Expansion (FAGE), exhibits several advantages: (i) Sampling at low pressure reduces the concentration of both O_3 and H_2O in the sampled air mass, as well as other trace gases, reducing the production of laser-generated OH as well as unwanted secondary chemistry (Stevens et al., 1994), (ii) The fluorescence lifetime of the excited OH radical is extended to hundreds of nanoseconds due to lower quenching rates, allowing temporal filtering of the weak OH fluorescence from the intense scattered laser-light. In addition, excitation of the OH radical at 308 nm instead of 282 nm further reduces the photolytic interference by a factor of approximately 30 due to a lower O_3 absorption cross section and a lower quantum yield for the production of $O(^1D)$ (Stevens et al., 1994). Note that the use of a high repetition-rate laser system that delivers low-energy pulses, but a high average power, also reduces the photolytic production of OH from each pulse. Instruments based on the FAGE design with resonant detection of OH at 308 nm have proven their ability to perform measurements of tropospheric OH by reducing the photolytic interference below negligible levels (Heard and Pilling, 2003).

Laser-Induced Fluorescence instruments as well as Chemical Ionization Mass Spectrometer (CIMS) and Differential Optical Absorption Spectrometer (DOAS) instruments have been used extensively to characterize the HO_x chemistry in a variety of different environments (Heard and Pilling, 2003). However, only a few investigations have focused on urban areas (Table 1). In addition to the local impacts of urban air quality, understanding the photochemistry of urban environments is important, as they may have a strong impact on regional air quality and global climate change (Molina and Molina, 2004).

In this paper we report the description of a HO_x instrument developed at Indiana University (IU-FAGE) based on the Fluorescence Assay by Gas Expansion technique and the resonant detection scheme at 308 nm. This instrument was first deployed as part of the Mexico City Metropolitan Area (MCMA) field campaign during March 2006, and successfully measured daytime OH and HO_2 concentrations. The qualitative behavior of HO_x concentrations during MCMA-2006 is examined and compared to observations from previous urban field campaigns. A more detailed analysis of the data, including model comparisons and a discussion of the radical budget will be presented in a companion paper (Dusanter et al.: Measurements of OH and HO_2 Concentrations during the MCMA-2006 Field Campaign – Part 2: Model comparison and radical budget, in preparation).

2 Instrument description

The IU-FAGE instrument takes advantage of the Laser-Induced Fluorescence Assay by Gas Expansion technique (LIF-FAGE) to probe the OH radical at low pressure together with excitation and detection of OH at 308 nm. IU-FAGE is equipped with a high repetition-rate laser system, a sampling cell for ambient air expansion, a reference cell for wavelength calibration, and a gated detection system.

2.1 High repetition rate laser system and laser-light propagation

A schematic of IU-FAGE instrument is shown in Fig. 1. The laser light is generated at a repetition rate of 6 kHz using a dye laser (Lambda Physik, Scanmate 1) pumped by the second harmonic of a pulsed Nd:YAG laser (Spectra Physics Navigator II YHP40-532Q). The primary emission of the dye laser was found to be optimum using a mixture of Rhodamine 640 in isopropanol. Approximately 7 W of laser light at 532 nm from the Nd:YAG laser produces 150–200 mW at 616 nm from the dye laser. The 616 nm emission is frequency doubled by a BBO (Beta Barium Borate) crystal, and the second

ACPD
8, 13689–13739, 2008

harmonic is separated from the fundamental by a system of prisms. The resulting laser beam at 308 nm exhibits a pulse-width of approximately 20 ns and an averaged laser power of 1–15 mW. A planoconvex lens, tilted to correct the laser beam astigmaticity, focuses the light onto an optical fiber launcher assembly employed to propagate the laser-beam to the sampling cell. Two different optical fibers (Thor Labs), 2 and 12 m long, are used depending on the experiment requirements. These fibers, with their optical launchers, exhibit respective transmittances of 45% and 37%.

Two quartz plates are positioned at an incident angle of 45° in the path of the laser beam after the BBO crystal. The first plate is used to deliver a small fraction of the UV light to a reference cell for wavelength calibration. The second plate allows monitoring the laser power at the output of the dye laser using a photodiode detector (UDT-555UV, OSI Optoelectronics) equipped with an interference filter (308 nm, ESCO products).

2.2 Sampling and reference cells

The sampling cell design is based on the Ground-based Tropospheric Hydrogen Oxides Sensor developed at Pennsylvania State University (Stevens et al., 1994; Mather et al., 1997; Faloona et al., 2004). The current version of IU-FAGE uses a single axis for successive measurement of OH and HO_2 radicals (Fig. 2). The sampling cell consists of a central aluminum cube 11.4 cm in length, a cylindrical inlet nozzle (5 cm diameter, 20 cm long) and a multi-pass cell (White design). Inner walls are anodized in order to minimize light scattering.

Ambient air is pumped through a flat pinhole approximately 1 mm in diameter and is expanded along the length of the nozzle. A loop injector is located downstream the sampling inlet to allow the addition of either nitric oxide (NO, Matheson, 99.8%) or perfluoropropylene (C_3F_6, Matheson, 99.8%). These gases are respectively used to convert ambient HO_2 into OH or to scavenge ambient OH before the detection axis. The loop was designed with radial holes pointing towards the center of the nozzle to improve the gas mixing and to avoid potential wall reactions. Three mechanical vacuum pumps (Leybold D16B, 20 $m^3 h^{-1}$) are connected in parallel to provide a flow

ACPD
8, 13689–13739, 2008

rate of 10 SLPM (Standard Liter Per Minute), allowing air to be refreshed rapidly at the detection axis. The internal pressure is kept at 5.3±0.2 hPa and is monitored at the bottom of the cell by an absolute capacitance gauge (MKS 0–10 Torr, better than 1% precision). The operating pressure was chosen for the following reasons: (i) an early FAGE instrument exhibited an unusual drop in sensitivity with an increase of the ambient water-vapor mixing ratio by operating the sampling cell at a lower pressure (Hofzumahaus et al., 1996; Creasey et al., 1997). This effect was attributed to radical scavenging on water clusters formed in the cold zone of the gas expansion. (ii) The sensitivity is strongly dependent on the operating pressure (Faloona et al., 2004); however, this dependence is minimized around 5.3 hPa and potential pressure changes during field measurements would induce less variation on the sensitivity than at other pressures.

A White-type multi-pass cell is used inside the sampling cell to improve the instrumental sensitivity by increasing the amount of generated fluorescence. It consists of three 1-in.-diameter mirrors, UV coated for high reflectivity (R>99.9%) at 308 nm with a base length of 250 cm. The entrance mirror has two cut-outs allowing the laser beam to enter and leave the sampling cell. The light delivered by the optical fiber is focused at the entrance mirror and is propagated 24 times through the sampled air mass before exiting the cell. The laser beam is then focused on an external photodiode detector for laser power monitoring (UDT-555UV, OSI Optoelectronics, interference filter at 308 nm, ESCO products). The multi-pass cell is designed with internal square openings allowing the laser beam to go back and forth between the mirrors while trapping scattered photons. Dry nitrogen is continuously flushed through each end of the multi-pass cell to avoid contamination of the mirrors.

A single-pass reference cell is employed to get the maximum spectral overlap between the laser emission and the OH transition. The cell is made out of aluminum and is equipped with 2 suprasil windows for laser beam access. A rotary pump (Leybold D16B, 20 $m^3 h^{-1}$) is used to keep the reference cell under vacuum and a high concentration of hydroxyl radical is produced by thermal dissociation of water-vapor at low

pressure using a hot alumel filament. The resulting OH fluorescence is collected by a Hamamatsu photomultiplier tube (H6180-01) equipped with an interference filter at 308 nm (ESCO products).

2.3 Gated photon-counting detection

The laser beam encounters the sampled air mass approximately 20 cm below the sampling point to insure that OH is probed when the rotational temperature has been thermalized to ambient temperature (Stevens et al., 1994; Kanaya et al., 2001). OH is probed under thermalized conditions for several reasons. (i) The low temperature in the cold zone of the gas expansion may lead to radical scavenging on water-clusters (Hofzumahaus et al., 1996; Creasey et al., 1997). (ii) The instrumental sensitivity depends on the Boltzmann distribution of OH and the quenching rates of the excited state by N_2, O_2 and H_2O. These parameters are strongly dependent on the temperature (Bailey et al., 1997) and geometry variations of the gas expansion may lead to OH sensitivity changes during field measurements. Probing OH in a thermalized region minimizes these issues.

The OH fluorescence is collected by an optical train (Fig. 2) at a right angle to the excitation beam through a solid angle that has been approximately doubled by using a concave mirror opposite the detector (10 cm diameter, 40 cm focal length, Melles Griot). Two coated lenses (f=75 mm, CVI Laser) allows careful imaging and spatial filtering of the fluorescence onto the detector. A band-pass filter centered at 308 nm (Barr Associates, transmission 65%, bandwidth 5 nm, OD>5 at other wavelengths), is inserted in the optical train to selectively reduce scattered photons from solar light, red-shifted fluorescence of the walls, and potential fluorescence of other chemical species.

The detection system is shown in Fig. 1 and is composed of a time-gated micro-channel plate photomultiplier tube (Hamamatsu R5916U-50), a preamplifier/discriminator (F-100T, Advanced Research Instruments) and a high-speed photon counter (SRS400, Stanford Research Systems). The intense laser light that is scattered when the laser is fired can saturate the micro-channel plate (MCP) and lead to

the generation of after-pulses which deteriorate the instrumental sensitivity (Creasey et al., 1998). To avoid detector saturation, the MCP gain is reduced by a factor of 10^5 during the laser pulse, and switched to the highest gain 60 ns after the laser pulse. The gain is kept high for approximately 1 μ s in order to collect most of the OH fluorescence, and is then reduced until the next laser-pulse. The signal from the MCP is amplified and filtered by a pulse-height discriminator that delivers TTL pulses for each detected photon. The photon counter is set with a timing gate using a delay and width for the 2 m long fiber of 130 and 260 ns after the laser pulse. These parameters were optimized to give the best signal-to-noise ratio by discriminating electronic noise and scattered laser-light against the weak OH fluorescence, and are different when the 12 m long fiber is used. Reflection of the laser light between the two ends of the fiber generates a second light pulse which occurs approximately 160 ns later than the main pulse, similar to that observed by Faloona et al. (2004). In order to reduce the detected scattered light from this secondary pulse, the MCP gain-switch and the photon counting gate are respectively delayed 70 and 90 ns later than that used for the 2 m long fiber.

The photoelectron pulses from the reference channel are detected and quantified by a counter on a National Instrument acquisition board (PCI-6024E). The reference channel signal (reference cell and associated electronics) was observed to cross-talk with the ambient channel (sampling cell and associated electronics) when the reference signal was too high. This issue was fixed by attenuating both the laser light propagated inside the reference cell and the amplitude of the photoelectron pulses. Two different tests are systematically performed during ambient OH measurements to insure that cross-talking between the counters has been efficiently eliminated: (i) S_{OH} in the sampling cell is alternatively measured with and without laser excitation inside the reference cell. (ii) S_{OH} is measured during air-zero tests when IU-FAGE is sampling clean air provided by a flow-tube interfaced on the top of the nozzle. During MCMA 2006, none of these tests showed a significant offset in the measured net OH signal.

ACPD
8, 13689–13739, 2008

2.4 Automation and field control

IU-FAGE is automated using a combination of GPIB, DAQ (National Instrument, PCI-6024E) and RS232 interfaces. A custom software program coded using LabView (National Instruments) allows monitoring the HO_x concentrations in real-time. The program includes several routines to acquire the excitation spectrum of OH, adjust the wavelength to maximize overlap between the laser emission and the OH transition, and perform periodic modulation cycles between on-resonance and off-resonance measurements. The program also switches between OH and HO_2 measurements by controlling the NO addition inside the sampling nozzle. A mass flow controller (MKS 1179A) is used to regulate the NO flow, and leakage during OH measurements is prevented by the internal valve of the flow controller and two additional solenoid valves connected in series. At the end of an HO_2 measurement, the valve of the flow controller is immediately closed, 10 s later the first solenoid valve located downstream of the flow controller is turned off, and the second solenoid valve is closed after another 10 s. In a similar manner, a flow of C_3F_6 can be added to check for potential photolytic interferences during OH measurements. This is discussed in detail in the HO_x-specificity section.

The time-resolution is controlled by the photon counter, which sums the detected photons from the ambient channel for 1 s and transfers the data to the computer. This event initiates the acquisition of 1 s averaged parameters such as the signal from the reference channel, the sampling cell pressure, the photodiode signals, NO and C_3F_6 flow rates, and the signals from ancillary monitors.

2.5 Measurement principle

The FAGE instrument is a non-zero background technique and the background signal must be measured to derive the net signal produced by the OH fluorescence. The procedure employed is based on successive modulation cycles during which the wavelength is successively tuned on-resonance and off-resonance with an OH transition. The on- and off-resonance measurements are usually acquired for 10 s in order to

ACPD
8, 13689–13739, 2008

catch the rapid variation of the background signal due to potential changes in the solar scattered light entering the nozzle (ambient light going through the nozzle).

The $Q_1(3)$ transition of OH at 308.1541 nm was chosen because the $Q_1(3)$-$Q_{21}(3)$-$P_1(1)$ triplet is easily identified and this transition exhibits one of the strongest absorption cross sections around 308 nm (σ=1.4×10^{-16} cm^2, P=1013 hPa, T=300 K) (Dorn et al., 1995). In addition, a rapid switching between $Q_1(3)$ and $P_1(1)$ allows for a check for potential spectral interferences from other ambient species. The fluorescence is a one photon process that is linear with both the laser power and the OH density, provided that the OH transition is not saturated. Stevens et al. (1994) observed a 10% saturation for the $Q_1(3)$ transition at 1.4 μJ/cm^2 (assuming a laser beam radius of 0.5 cm). The maximum laser power of 15 mW produced by the IU-FAGE instrument leads to an average value of approximately 6.5 mW of UV light inside the sampling cell when the 2 m long fiber is used. The laser fluence calculated for the maximum laser power is 1.1 μJ/cm^2 (beam radius of 0.5 cm), below the 10%-limit determined by Stevens et al. (1994).

Figure 3 displays a segment of raw data recorded on 15 March 2006 during the MCMA-2006 field campaign. One half of the measurement time is devoted to measuring the background signal, while the remaining time is dedicated to measuring the on-resonance signal. The off-resonance signal is an average of the two backgrounds surrounding the on-resonance measurement ($\lambda_{on-resonance}$-0.004 nm and $\lambda_{on-resonance}$+0.004 nm). Tests performed in the laboratory have shown that less than 1% of the on-resonance OH signal was measured at the background wavelengths under the working conditions.

The net OH signal (S_{OH}) is inferred from subtracting the off-resonance signal from the on-resonance signal. The advantage of measuring the background as an averaged surrounding off-resonance signal is twofold: (i) The laser power varies slightly with wavelength, which can lead to small differences in the background signal between the on- and off-resonance measurements. This may lead to a miscalculation of the net OH signal if the background signal is only measured on one side of the OH transition,

especially if the background signal is largely due to scattered laser-light. (ii) Comparing the two surrounding background signals allows checking for potential spectral interferences which may be induced by other fluorescing species. An interesting example can be found in Martinez et al. (2004). The authors observed that naphthalene exhibit a transition at a slightly longer wavelength than the $Q_1(2)$ transition of OH and fluoresce around 308 nm. Potential spectral interferences in the measurements presented here are discussed in the HO_x-specificity section.

Hydroperoxy radical measurements are based on the rapid gas-phase reaction of HO_2 with nitric oxide and subsequent detection as OH (R3):

$$HO_2 + NO \rightarrow OH + NO_2 \quad \text{(R3)}$$

$$OH + NO + M \rightarrow HONO + M \quad \text{(R4)}$$

A flow of pure NO (Matheson, better than 99% purity) is added through a loop injector located just below the sampling point after passing though an ascarite trap. The optimum NO flow (1 SCCM) used to convert the HO_2 radicals before the detection axis is a trade-off between the conversion of HO_2 into OH and the removal of OH by reaction with NO (R4). The fraction of HO_2 (C_{HO2}) converted into OH is measured during calibration experiments. Although the transit time to the detection axis is long enough to convert most of the HO_2 radicals, the RO_2 chemistry is slow enough to avoid the HO_2 formation through (R5–R6) (Stevens et al., 1994):

$$RO_2 + NO \rightarrow RO + NO_2 \quad \text{(R5)}$$

$$RO + O_2 \rightarrow R'O + HO_2 \quad \text{(R6)}$$

When NO is added to the sampled air stream, the sum (background + net OH + net HO_2) is measured. The net HO_2 signal (S_{HO_2}) is derived from the subtraction between the net OH signal with NO added and the net OH signal without NO.

The radical concentrations are calculated by inverting Eq. (1) and (2), and require the measurement of S_{OH}, S_{HO_2} and the laser power P_w. It also requires the calibration

of the detector response towards OH (R_{OH}) and HO_2 (R_{HO_2}) which are discussed in the calibration section. R_{OH} represent the number of photon counts per second produced per OH radical and normalized to 1-mW of laser power. The detector response towards HO_2 (R_{HO_2}) is the product of R_{OH} and the fraction of HO_2 converted into OH (C_{HO_2}) prior the detection axis ($R_{HO_2}=R_{OH}\times C_{HO_2}$).

$$S_{OH}=[OH]\times R_{OH}\times P_w \quad (1)$$

$$S_{HO_2}=[HO_2]\times R_{HO_2}\times P_w \quad (2)$$

The instrumental stability is largely governed by the stability of the laser intensity. Slow drifts are tracked during measurements by monitoring the laser power at the exit of both the dye laser (UV_{dye}) and the white cell (UV_{cell}). The ratio UV_{cell}/UV_{dye} is used to track the transmission of the laser light through the optical fiber and the cleanliness of the optics inside the white cell.

2.6 Instrument calibration

The accuracy of in situ measurements of OH and HO_2 radicals in the atmosphere is critically dependent on the accuracy of the calibration factor and the potential changes which may occur during field measurements. The sensitivity towards OH depends on the excitation rate (ER) of OH in the rotational level being probed, on the fluorescence yield (FY) of the OH excited state and on the collection efficiency (CE) of the resulting fluorescence (Stevens et al., 1994; Holland et al., 1995; Kanaya et al., 2001):

$$R_{OH}=f\left[ER\left(L,\nu,\Delta\nu_D,\Delta\nu_L,P_w,P_{cell},P_{amb},T\right),FY\left(\tau_{rad},k_{q_i},[M_i]\right),CE\left(\Omega,T_v,\eta_v,f\right)\right] \quad (3)$$

The excitation rate (ER) represents how many OH radicals are brought to the excited state per unit of time. This term is a function of the length of the laser beam overlapping the ambient air stream, L, the operating wavelength, ν, the full widths at half maximums of the molecular (Doppler, $\Delta\nu_D$) and laser ($\Delta\nu_L$) lineshapes, the averaged laser power,

P_w, the pressure inside and outside the sampling cell, P_{cell} and P_{amb}, and the rotational temperature at the detection axis, T. The collection efficiency (CE) represents the fraction of fluorescence collected by the optical train and recorded by the photon counting system. This term depends on the fraction of the solid angle imaged on the detector, Ω, the transmittance of the optics, T_v, the quantum efficiency of the MCP, η_v, and the fraction of the pulses emitted during the counting gate period, f. With the exception of average laser power, both the excitation rate and the collection efficiency depend on parameters that are kept under control and do not vary during field measurements, except the excitation rate which depends linearly on the averaged laser power. However, simultaneous monitoring of the laser power during HO_x measurements allows tracking the excitation rate (ER) and thus R_{OH}.

The fluorescence efficiency (FE) is the ratio of the natural radiative lifetime, τ_{rad}, and the total lifetime of the OH excited state, τ:

$$FE = \frac{\tau_{rad}}{\tau} \tag{4}$$

The total lifetime depends on τ_{rad} and on the collisional deactivations due to the species q_i which quench electronically excited OH by inelastic scattering at a rate k_{q_i}:

$$\tau = \tau_{rad} + \frac{1}{\sum_i k_{q_i}[q_i]} \tag{5}$$

The fluorescence yield, and thus R_{OH}, depends on the operating pressure and the chemical composition of the sampled air mass. The most efficient quenchers of the OH excited state in ambient air are N_2, O_2 and H_2O. Constant atmospheric O_2 and N_2 mixing ratios as well as the negligible variation of the internal pressure under normal operating conditions do not cause variation of the quenching rates. However, the water mixing ratio is highly variable in the troposphere (1–3%) and care must be taken to calibrate the dependence of R_{OH} toward the water concentration. During field measurements, simultaneous monitoring of absolute humidity allows correction of R_{OH} for the quenching of the fluorescence yield from water-vapor.

The calibration procedures employed to measure R_{OH} and R_{HO_2} have been described in detail elsewhere (Dusanter et al., 2008) and only information relevant to the HO_x calibration for MCMA-2006 is given here. Calibrations were performed using two techniques based on fundamentally different approaches. Calibrations using the steady-state O_3-alkene technique were done before, during and after the MCMA campaign, while calibrations using the water-vapor UV-photolysis technique were done after the MCMA campaign.

The O_3-alkene technique relies on the production of a steady-state concentration of OH during the ozonolysis of trans-2-butene in a flow tube at atmospheric pressure. During a calibration, S_{OH} is measured at various alkene concentrations for a constant ozone concentration. R_{OH} is inferred from its relationship with the intercept of a linear regression between $1/S_{OH}$ and 1/[trans-2-butene] and the values of the rate constants involved in the OH steady-state calculation (Hard et al., 2002; Dusanter et al., 2008). The water-vapor UV-photolysis technique takes advantage of the photolysis of water-vapor at 184.9 nm in a calibrator at atmospheric pressure. The water-vapor photolysis leads to the production of an equal amount of OH and HO_2 radicals. The concentration of OH radicals is determined using O_2 actinometry to derive the lamp flux and the photolysis time (Dusanter et al., 2008). Inside the calibrator, OH and HO_2 radicals can be lost through self- and cross-reactions and on the wall of the calibrator. The loss of each radical is measured during the calibration procedure and the calculated concentrations are corrected to reflect the concentration of radicals entering the instrument (Dusanter et al., 2008).

The sensitivities derived from the steady-state O_3-alkene technique were found to be consistently lower than that derived from the water-vapor UV-photolysis technique by approximately 40%. Although this difference is within the experimental uncertainties of the techniques, there are a number of possible explanations for this difference (Dusanter et al., 2008). A likely reason for the discrepancy between the techniques is a systematic error associated with the O_3-alkene calibration technique which may be the result of an OH production time-scale that is different between the calibration ex-

periments (140–210 ms) and the scavenger experiments used to derive OH yields from O_3-alkene reactions (a few minutes to hours) (Atkinson and Aschmann, 1993; Fenske et al., 2000; Kroll et al., 2001b). The OH yields published in the literature, measured at long reaction times, may be higher than the OH yield produced in the calibration system at short reaction times (Kroll et al., 2001a). As a result, using the reported OH yield may lead to an underestimation of R_{OH}. Because of the uncertain O_3-alkene chemistry and the time dependence of the OH yield, only calibrations performed with the water-vapor UV-photolysis technique were used to derive R_{OH} for the IU-FAGE instrument (Dusanter et al., 2008).

Prior to the MCMA-2006 field campaign, laboratory calibrations performed with a 2 m long optical fiber using the O_3-alkene calibration technique led to a measured R_{OH} of 2.1×10^{-6} cts/s/cm^{-3}/mW in dry air. Similar calibrations were performed using a 12 m long fiber and led to a measured R_{OH} of 9.0×10^{-7} cts/s/cm^{-3}/mW in dry air, which is approximately 2.3 times lower than that obtained from the shorter fiber. This difference is due to a lower transmittance of the laser light through the longer fiber and the use of a delayed counting gate to avoid background scatter due to reflection of the laser off the ends of the fiber (see below).

During the MCMA-2006 campaign, the IU-FAGE instrument was set-up with the 12 m long optical fiber and calibrated using the O_3-alkene technique. Fig. 4 displays six field calibrations and shows the stability of R_{OH} throughout the campaign. The averaged sensitivity measured using this calibration technique was $R_{OH}=8.8\times10^{-7}$ cts/s/cm^{-3}/mW in dry air, similar to the calibrations performed before the campaign. This value of R_{OH} for the MCMA-2006 campaign was then corrected to account for the systematic difference of 40% observed between the water-vapor UV-photolysis technique and the steady-state O_3-alkene technique. R_{OH} was also corrected for its water-dependence using additional calibrations performed after the campaign (Dusanter et al., 2008). Uncertainties in R_{OH} and R_{HO_2} from the water-vapor UV-photolysis calibration technique are respectively 17% and 18% (Dusanter et al., 2008), while the precision in the measurements of R_{OH} using the O_3-alkene technique is 7%.

Assuming an additional error of 10% to correct for the systematic difference between the calibration techniques and a quadratic propagation of errors, the uncertainties on R_{OH} and R_{HO_2} for the MCMA campaign are respectively 21% and 22%.

2.7 Specificity of the HO_x measurements

Spectral interferences in the measured OH signal may be caused by other fluorescing species, which can be excited and detected around 308 nm. Only species exhibiting a resolved excitation spectrum can interfere with HO_x measurements due to the fine rotational structure of OH and the on/off-resonance procedure used to derive S_{OH}. The fluorescence generated by species that exhibits broad absorption features is discriminated from the OH fluorescence during the measurement sequence when the laser wavelength is adjusted on- and off- resonance with the narrow OH spectral line. The same amount of spurious fluorescence is recorded during on- and off- measurements and potential interferences are automatically subtracted when the net OH signal is derived. However, chemical species such as naphthalene and formaldehyde exhibit resolved excitation spectrums near 308 nm and may interfere with OH measurements. Naphthalene was recently observed to interfere during background measurements when the $Q_1(2)$ transition of OH is employed (Ren et al., 2004). However, published naphthalene excitation spectrums around $Q_1(2)$ and $Q_1(3)$ show that $Q_1(3)$ is free of interferences (Martinez et al., 2004). Ren et al. (2004) investigated potential spectral interferences on GTHOS and concluded that formaldehyde does not interfere for OH measurements using the $Q_1(2)$ transition. It is worth noting that the instrumental response to formaldehyde may be somewhat different for the $Q_1(3)$ transition. To our knowledge, no other spectral interferences have been reported in the literature for the resonant detection scheme of OH at 308 nm. In the future, instrumental tests will be performed during field measurements to investigate whether potential spectral interferences are presents. The spectral properties of the fluorescing species, excitation spectrum and lifetime of the excited state, can be compared to the expected OH values to provide strong evidence that the detected signal arises solely from the OH radical.

ACPD
8, 13689–13739, 2008

Unfortunately, the sensitivity of the instrument prevented implementation of these tests during the MCMA-2006 field campaign.

Additional interferences with measurements of ambient OH radicals can arise from OH radicals generated in the low-pressure region of the FAGE apparatus. Chemical species that absorb the laser light during measurements may decompose and produce OH directly (HONO→ OH+NO for example) and indirectly (the O_3-water interference mentioned above). This artificial OH is then detected within the same laser pulse that produced it. Ren et al. (2004) investigated potential photolytic interferences from HONO, H_2O_2, HNO_3 and acetone on the GTHOS instrument and concluded that none of these species were able to generate significant interferences.

Photolytic production of OH can be investigated during field measurements using two different on-line tests: (i) In contrast to the detection of ambient OH, which is a one photon process, the detection of laser-generated OH requires two photons to successively produce and detect an OH molecule. The one-photon process will exhibit a linear dependence with the averaged laser power, while the two-photon process will show a quadratic dependence. In order to determine whether laser-generated OH is produced in the detection region, the OH concentration is successively measured at various laser powers, providing that ambient OH concentrations do not vary significantly between the measurements. (ii) A second test is based on chemical modulation of OH by adding a scavenger (C_3F_6) during the sampling stage (Dubey et al., 1996). The scavenger concentration is adjusted to remove ambient OH prior to the air sample reaching the detection region. Laser-generated OH produced and detected within the same laser pulse will not be removed efficiently due to the short reaction time and can be easily identified.

Thermal decomposition of an unstable species inside the low-pressure cell may also produce OH. A possible example is the unimolecular decomposition of Criegee intermediates produced from the reaction of O_3 with alkenes, producing OH radicals at low pressure (Kroll et al., 2001a). This spurious OH would exhibit a linear dependence with the laser power. As a result this interference can not be detected by changes in the

laser intensity. However, a change in the efficiency of the chemical modulation could indicate the production of OH from a non-photolytic source.

The IU-FAGE instrument was equipped with the chemical modulation test before the MCMA campaign, with addition of C_3F_6 through the same injector used for NO injection. However, difficulties associated with the NO injection system during the campaign required disabling the C_3F_6 injection system. The absence of this automated test makes it difficult to rule out interferences during the MCMA campaign. However, several points suggest that the level of such interferences were low compared to ambient OH concentrations: (i) The IU-FAGE instrument is based on a similar design than GTHOS (Faloona et al., 2004), which was deployed in a similar polluted environment without interference issues during MCMA-2003 (Shirley et al., 2006). In addition, the IU-FAGE instrument uses a lower laser power than GTHOS to detect OH, suggesting lower potential photolytic interferences. (ii) Tests performed before the MCMA-2006 campaign (including C_3F_6 tests on ambient measurements) suggest that the IU-FAGE instrument was free of photolytic interferences. (iii) Over the course of the campaign, the laser power decreased from 15.8 to 2.2 mW. If a laser generated interference was present, it would be expected that its contribution would decrease by a factor of approximately 50 during the campaign. However, measured OH concentrations did not exhibit a significant trend as the laser power decreased (Fig. 5), strongly suggesting that the measurements are free of photolytic interferences.

An additional interference was present during HO_2 measurements due to the addition of NO inside the sampling cell. We observed a signal showing a power dependence with the laser power and a linear dependence with the NO concentration, characteristic of a multi-photon photolytic process. This interference, probably caused by photolysis of unknown impurities in the NO mixture, has not been identified yet but has been quantified during the MCMA campaign by performing zero-air tests. A flow-tube was attached to the sampling nozzle and the laser-generated OH was measured in clean air with NO flowing through the injector. Tests performed showed an excellent linearity between the detected signal and the NO flow. The net signal was normalized to

1-SCCM of NO and plotted against the laser power as shown in Fig. 6. The signal exhibits a clear dependence on the laser power, characterized by an exponential factor of 3.80±0.07(1σ, N=36 values). The exponential factor is higher than the expected quadratic dependence of a simple photolytic production of OH such as the O_3-water interference. Further laboratory tests will be performed to resolve this issue. However, the calibration curve shown in Fig. 6 allows quantification of the OH interference produced during HO_2 measurements, and this curve was used to correct the net HO_2 signal measured during the MCMA campaign. Corrections were in the range 5–60% on a daily average with the highest impact for days when HO_2 concentrations were low and a high laser power was used. In general, this correction was usually below 35%. The additional error due to this interference was included in the estimates of the precision of the HO_2 measurement.

2.8 Instrument performance

The overall performance of IU-FAGE in terms of precision and limit of detection depends on the calibrated sensitivity, the stability of the laser power, and the various sources of noise that contribute to the background signal. The latter is detected in absence of OH fluorescence and is a combination of dark noise, electronic noise, and scattered photons from solar light and the laser beam. Dark noise is inherent to the detector and its contribution to the background signal is negligible. Electronic noise was reduced by careful design of the detection system and its contribution does not limit the performances of IU-FAGE. Prompt scattering of the excitation photons is the primary component of the background signal that deteriorates the detection limit of OH. Scattered photons from gaseous molecules (Rayleigh), particles (Mie) and reflections on the wall of the sampling cell are minimized by working at low pressure, careful baffling of the laser path, anodized inner surfaces and a gated detection system.

Instrument performance can be expressed using three quantities: the measurement precision, the detection limit and the total uncertainty. The precision is governed by rapid variations of the background signal due to laser power fluctuations, changes in

ACPD
8, 13689–13739, 2008

Rayleigh and Mie scattering efficiency, and changes in solar scattered light. The precision, σ_p, is defined by the standard deviation of the background signal integrated during t seconds at N samples/second:

$$\sigma_p = \frac{\sqrt{2}\sigma_{\text{bkg}}}{\sqrt{Nt}} \quad (6)$$

Equation (6) assumes that the number of points acquired ($N \times t$) is similar for the on-resonance and the off-resonance signals as shown by the factor of $2^{1/2}$. Using photon counting techniques, the standard deviation of the background signal follows a Poisson distribution and σ_{bkg} is equal to the square root of the background signal. However, investigations of the IU-FAGE background signal have shown that its distribution does not follow Poisson statistics. Figure 7 shows two segments of data taken during laboratory and field measurements, and shows that the background signal distribution is better represented by a Normal distribution. The reason for this is not well understood and further investigations will be performed to resolve this point. As a consequence, the precision of our measurements for the MCMA campaign was calculated using Normal statistics. It is worth noting that using a Poisson distribution would improve the measurement precision but would lead to an obvious underestimation of the measurement error.

The detection limit is the lowest OH concentration required to observe a net OH signal that is above the precision for a given signal to noise ratio (SNR):

$$[\text{OH}]_{\text{min}} = \text{SNR} \times \frac{\sigma_p}{R_{\text{OH}} P_w} \quad (7)$$

The total uncertainty for an OH measurement depends on the precision (σ_p), the uncertainty of the calibrated sensitivity R_{OH}, the uncertainty of the R_{OH} water-dependence and the uncertainties of the measured ambient water mixing ratios and laser power. Laboratory characterizations performed before the MCMA campaign shown that the IU-FAGE instrument, set-up with the 12 m long fiber, is capable of detecting

3.9×10^5 molec cm^3 at a signal to noise ratio of 1, an averaged laser power of 10 mW and a signal integration time of 5 min (on-resonance+off-resonance measurements). The calibration accuracies (1σ) are ±17% for OH and ±18% for HO_2 using the water photolysis calibration technique. However, during the MCMA-2006 campaign, the IU-FAGE instrument was prone to a large, unknown electronic noise which deteriorated the instrument performance. The observed minimum detectable varied from 5.0×10^5 to 2.6×10^6 molec cm^{-3} for a laser power ranging between 15 and 2 mW and an integration time of 30 min. Improved shielding and grounding of the detection system will be employed for future field deployments to reduce this potential interference.

3 Deployment of IU-FAGE during MCMA-2006

The Mexico City Metropolitan Area 2006 (MCMA-2006) field campaign was one of four components of MILAGRO (Megacity Initiative: Local And Global Research Observations) intended to collect scientific information on the impact of megacity emissions on local, regional and global scales. The Mexico City Metropolitan Area was chosen as a case study for several reasons. Mexico City is the second largest megacity in the world and is characterized by high emissions of VOCs and NO_x. In addition, frequent thermal inversions and the surrounding mountains limit the dispersion of pollutants. Mexico City lies at a sub-tropical latitude and an elevated altitude of 2240 m, resulting in an active photochemical environment. As a result, chemical processing of the primary pollutants in the MCMA basin gives rise to secondary pollutants such as O_3, whose concentration exceed air quality standards more than 300 days a year (Raga and Raga, 2000; Molina and Molina, 2002). More information about recent MCMA field studies can be found in Molina et al. (2007) and references therein.

Only details pertinent to the HO_x measurements performed by the IU-FAGE instrument are given in the following section. Qualitative observations are provided to help understand the behavior of HO_x concentrations in polluted environments. Comparisons between model-predicted and measured HO_x concentrations and an assessment of the

radical budget during MCMA-2006 will be presented in a separate publication (Dusanter et al.: Measurements of OH and HO_2 Concentrations during the MCMA-2006 Field Campaign: Part 2–Model Comparison and Radical Budget, in preparation).

3.1 HO_x measurements

Atmospheric OH and HO_2 concentrations were measured at the Instituto Mexicano del Petroleo (T0 site) between 14 and 31 March. The laser system and associated electronics were located inside an annex on the roof of Building 32 as shown in Fig. 8. The sampling cell was located on the roof of this annex and was set-up using the 12 m long optical fiber. Additional collocated measurements of radiative parameters and longer lived species, characterizing HO_x sources (photolysis rate constants, O_3, HCHO, CH_3CHO, HONO, CHOCHO, HNO_3), sinks (NO_x, SO_2, CO, VOCs), and meteorological parameters were also measured at this site by other institutions.

As mentioned in the Instrument performance section, the precision of the HO_x measurements during the campaign was degraded by electronic noise at this site, and an averaging time of 7–30 min was necessary to achieve a reasonable detection limit ranging from 5.0×10^5 to 2.6×10^6 molec cm^{-3} at SNR=1 for OH. HO_2 concentrations were 10–100 times higher than OH and an averaging time of 15 s is sufficient to get a detection limit in the range 4.4×10^6 to 2.8×10^7 molec cm^{-3}. OH and HO_2 were not measured simultaneously, as only one detection axis was used to measure both radicals. HO_2 was measured for 15–s every 15 min (14–15 March) and every 8 min (16–31 March) and OH was measured during the remaining time using 10 s modulation cycles. The calibration accuracies (1σ) are 21% for OH and 22% for HO_2, taking into account the additional error introduced by the correction from the systematic difference observed between the steady-state O_3-alkene and the water-vapor UV-photolysis calibration techniques, as discussed in the Calibration section.

The time series of measured OH concentrations and its median profile for all measurements are displayed in Figs. 9–11, together with measured J(O^1D) values. These figures show that OH exhibits a diurnal pattern, which closely follows the so-

ACPD
8, 13689–13739, 2008

lar actinic flux. The maximum OH concentration observed from day to day varied between 2.0×10^6 and 1.5×10^7 molec cm^{-3}. On a median basis, OH peaked near 4.6×10^6 molec cm^{-3} at noon (CST) and displayed an asymmetric profile with higher concentrations measured at this site during the morning hours (Fig. 9). In addition, high levels of OH are clearly observed on 16, 18 and 21 March between 09:30–11:00 a.m. (Fig. 9). This suggests that efficient HO_x sources and/or a fast radical propagation under the high NO_x conditions of the MCMA exist during the morning hours. This is consistent with the intense morning photochemistry observed during MCMA-2003 (Shirley et al., 2006; Volkamer et al., 2007). OH concentrations decrease with $J(O^1D)$ in the late afternoon and remain at a significant level of $0.7–1.5\times10^6$ molec cm^{-3} between 05:00 and 07:00 p.m. CST. This may be the result of the HO_2 conversion into OH through its reaction with NO and/or the ozonolysis of unsaturated compounds which are known to yield OH, HO_2 and RO_2 radicals (Paulson and Orlando, 1996).

A time series and the median diurnal profile of the measured HO_2 concentrations are also displayed in Figs. 9–11. The dependence of HO_2 concentrations on the solar actinic flux is less evident than that for OH. The maximum daily HO_2 concentration ranged from 5.6×10^7 to 4.5×10^8 molec cm^{-3}. In addition, peak concentrations up to 6.5×10^8 molec cm^{-3}, were also observed on 28 and 31 March during morning hours. The diurnal median profile of HO_2 peaks at 1.9×10^8 molec cm^{-3} and occurs approximately one hour later than OH. The later peak of HO_2 in urban environments with respect to $J(O^1D)$ has been observed previously in several studies and is likely related to high NO_x emissions during the morning rush-hour suppressing the concentrations of HO_2 as well as O_3 (Holland et al., 2003; Martinez et al., 2003; Ren et al., 2003a; Shirley et al., 2006). Figure 12 also displays measurements of NO, NO_2 and O_3 sampled within 50–100 cm of the IU-FAGE nozzle. The median NO mixing ratio was more than 200 ppb around 07:00 a.m. and decreased slowly during the morning and early afternoon.

Photolysis of O_3 at short wavelengths and the subsequent reaction of the photoproduct $O(^1D)$ with water-vapor (R1–R2) is the major source of RO_x radicals in the remote-

rural troposphere and J(O^1D) can be considered as an indicator for the total photolytic production of odd hydrogen radicals. However, photolysis of other oxygenated species such as HONO, glyoxal, methylglyoxal and other dicarbonyl species can also contribute to the RO_x production in urban environments. The contribution of these species to the production of RO_x have been found to be important relative to O_3 photolysis in the MCMA (Volkamer et al., 2007). Note that like HONO, these species are photolysed at wavelengths longer than 330 nm, and as a result J(HONO) is expected to be a better proxy than J(O^1D) to describe the total photolytic production of RO_x in this environment. Figure 13 displays a correlation plot between measured OH and J(HONO) that illustrates the OH dependence on the photolytic production of radicals in MCMA-2006. The low correlation coefficient (R^2=0.199) indicates that only 19.9% of the variance of OH can be explained by variations in J(HONO). Note that a plot of OH versus J(O^1D) provides an even lower correlation coefficient, similar to that observed by Kanaya et al. (2007) in Tokyo when J(NO_2) is used instead of J(HONO) (Kanaya et al., 2007). A large part of this variance can be attributed to the OH measurement precision and to a lesser extent to the variability of the atmospheric chemical composition (HONO, dicarbonyl species, O_3, NO) for similar J(HONO) values. The positive intercept may suggest non-photochemical processes such as O_3-alkene reactions which can produce HO_x radicals when J(HONO) is low, or a bias due to higher HONO concentrations in the early morning. Figure 13 also displays OH measurements performed under high and low NO_x conditions. The similar OH concentrations observed between these the two regimes for similar J(HONO) values suggest that OH concentrations are well buffered under the polluted conditions of MCMA-2006.

Under the high concentrations of NO_x observed during MCMA-2006, both OH and HO_2 are expected to decrease with increasing NO under conditions where the production rate of the radicals is constant (Martinez et al., 2003; Ren et al., 2003a). In the MCMA, the morning production of HO_x is mainly controlled by photolysis of HONO and to a smaller extent by photolysis of glyoxal, methyl glyoxal and unsaturated dicarbonyl species (Volkamer et al., 2007; Dusanter et al.: Measurements of OH and HO_2

Concentrations During the MCMA-2006 Field Campaign: Part 2–Model Comparison and Radical Budget, in preparation). However, in the MCMA NO_x concentrations and J-values are coupled together. High NO_x concentrations observed in the early morning are characterized by low J-values and low NO_x concentrations by higher J-values in the late morning-early afternoon. In order to investigate the HO_x/NO dependence, daily 30 min median OH and HO_2 concentrations were normalized to the measured 30 min median J(HONO) and multiplied by an average J(HONO) calculated from 08:30 a.m. to 06:30 p.m. A similar procedure was then employed to normalize the resulting HO_x concentrations to the measured HONO concentrations in order to normalize variations in the measured HO_x concentrations from HONO photolysis. $[OH]_{normalized}$ and $[HO_2]_{normalized}$ are plotted as a function of [NO] in Fig. 14. Only HO_x measurements performed at NO mixing ratios above 8 ppb are displayed in this Fig. NO mixing ratios below 8 ppb were characteristic of measurements performed in the late morning and afternoon where other sources of HO_x, such as the photolysis of formaldehyde, cannot be normalized by J(HONO). As can be seen in Fig. 14, both OH and HO_2 decrease with increasing NO as expected for high NO_x environments.

3.2 Comparison with previous urban measurements

Table 1 is a chronologic compilation of the field campaigns performed in urban and sub-urban environments that include HO_x measurements. Nine of the twelve studies were performed during spring-summer months, while only three studies focused on the photochemistry occurring in winter. Measurement-model comparisons have been performed using either comprehensive reaction mechanisms such as the Master Chemical Mechanism (MCM), or lumped chemical mechanisms such as the Regional Atmospheric Chemical Mechanism (RACM). Agreement between modeled and measured HO_x concentrations ranged between an underprediction by a factor of 2 for OH (PUMA) and 6 for HO_2 (PMTACs winter campaign), and an overprediction by factors of 1.5–2 for OH (LAFRE, BERLIOZ) and 1.4 for HO_2 (BERLIOZ), with occasional agreement for both OH and HO_2 (MCMA-2003). This sparse agreement between measure-

ment and model illustrates the difficulty in characterizing the complex HO_x chemistry of polluted environments.

Table 1 indicates that the production of HO_x radicals under polluted conditions is sometimes controlled by the photolysis of O_3 (BERLIOZ, SOS), as in remote environments. However, processes such as HONO photolysis (LAFRE, PMTACs) and non-photolytic O_3-alkene reactions (PUMA) can also dominate HO_x production in urban environments. The wide variety of HO_x sources and sinks involved in urban environments makes it difficult to determine the radical budget in these areas. However, similar to the results shown in Fig. 13, which suggest that OH concentrations are well buffered within the same site, Table 1 suggests that OH concentrations are also buffered on a larger scale under a wide range of polluted conditions. Measured OH concentrations for the summer campaigns range from 2 to 9×10^6 cm^{-3}, with the exception of PMTAC and SOS where OH concentrations as high as 20×10^6 cm^{-3} were observed on some days. It is interesting to note that high nighttime OH and HO_2 concentrations were also frequently observed during these two campaigns, in contrast to the other urban field measurements. This may suggest the contribution of additional HO_x sources for the latter two studies. This qualitative behavior suggests that the increased primary loss of OH, due to increasing NO_x and VOCs concentrations, is often offset by higher secondary production rates of HO_x radicals due to photolytic reactions of oxygenated species, reactions between O_3 and alkenes and the production of OH from the rapid HO_2 conversion by NO. In contrast, HO_2 concentrations are much more sensitive to the NO_x levels, due to the rapid HO_2+NO reaction, and act as a buffer for OH.

The HO_2/OH ratio reflects the partitioning between OH and HO_2, which depends on the processes that interconvert the radicals. In contrast to absolute concentrations of HO_x, this ratio does not depend on the production and termination rates of the radicals. As a consequence, HO_2/OH is an interesting indicator of the cycling of RO_x (OH+HO_2+RO_2) radicals that can be used as a measure of the efficiency of radical propagation. Measured HO_2/OH ratios as a function of NO are displayed in Fig. 15. Note that OH and HO_2 were not measured simultaneously and for these calculations

ACPD
8, 13689–13739, 2008

OH was averaged for 30 min around each HO_2 measurement (15 min before and after). HO_2/OH is expected to depend on NO_x and VOC concentrations and is expected to decrease with increasing NO because of the fast conversion of HO_2 into OH, Eq. (8):

$$\frac{[HO_2]}{[OH]} \approx \frac{\Sigma \text{Rate of reactions}(OH \rightarrow HO_2)}{\Sigma \text{Rate of reactions}(HO_2 \rightarrow OH)} \approx \frac{k_{OH+VOC}[VOC]+k_{OH+CO}[CO]+k_{OH}+O_3[O_3]}{k_{HO_2+NO}[NO]+k_{HO_2+O_3}[O_3]} \quad (8)$$

Observed HO_2/OH ratios varied from 1 to 120 during MCMA-2006, while measured NO mixing ratios were in the range 1–120 ppb for these calculations. These ratios are similar to that measured in previous campaigns (Table 1) and appears to show the expected NO dependence. It is interesting to compare the results from MCMA-2003 and 2006 where the HO_2/OH ratios were measured in the same city, but at different locations and 3 years apart. The measured ratios during 2006 are generally smaller than that measured in 2003 for a similar NO mixing ratio (typical HO_2/OH ratios of 40 at 10 ppb of NO during MCMA-2003). This result is consistent with the lower concentrations of CO observed during 2006 (median peak CO of 2600 ppb in 2003 (Shirley et al., 2006) compared to a median 1600 ppb for CO in 2006), although the total level of VOCs was similar during the two campaigns (median peak of 1500 ppbc in 2003 (Shirley et al., 2006) compared to a median of 1600 ppbc for VOCs in 2006). However, median NO_x levels were generally 3 times lower in 2003 compared to 2006.

The instantaneous rate of O_3 production from HO_2, $P(O_3)$ in Eq. (10), is driven by radical propagation and is also an indicator of the cycling between OH and peroxy radicals.

$$P(O_3) = k_{HO_2+NO}[HO_2][NO] - k_{OH+NO_2}[OH][NO_2] \quad (9)$$

Figure 16 displays $P(O_3)$ due to HO_x radical chemistry calculated from 30 min median measurements of HO_x and NO_x between 14 and 31 March. $P(O_3)$ was as high as 80 ppb/hr in the early morning (8:30–10:00 CST) and decreased to 31 ppb/hr around noon, reaching a minimum of 3–4 ppb/hr in the late afternoon (17:00–18:00 CST). The high $P(O_3)$ values observed before solar noon are consistent with those observed in

other urban environments (Martinez et al., 2003; Ren et al., 2003b; Shirley et al., 2006). $P(O_3)$ values calculated for MCMA-2003 (Shirley et al., 2006) were about a factor of two lower than that for 2006, while peak median OH and HO_2 concentrations were approximately 1.5 and 3.9 times higher in 2003, also consistent with the lower NO_x levels observed in 2003 compared to 2006. Assuming that the HO_x production rates are similar, these results may suggest a larger sink of HO_x radicals in 2006 compared to 2003.

4 Conclusions

A new instrument capable of measuring tropospheric OH and HO_2 concentrations by laser-induced fluorescence at low pressure has been developed and was deployed for the first time during the MCMA-2006 field campaign. Although experimental difficulties degraded the instrument's performance, diurnal concentration profiles of OH and HO_2 were successfully measured in Mexico City. At the present time, the minimum detectible OH is limited by the scattered laser light inside the sampling cell. Inorganic black coating and a lower internal pressure will be tested to improve the detection limit. In addition, the laser system and the propagation of the laser light will be optimized to increase the laser power inside the sampling cell. An on-line calibration system will be added to track potential daily variations of the instrument sensitivity during the day. Several automated tests will also be added in order to check for potential interferences during field measurements. First, measurements will be systematically performed as a function of laser power to test for laser generated OH. Second, measurements will be performed using both the $Q_1(3)$ and the $P_1(1)$ transition of OH to check for potential spectral interferences on a specific transition, in addition to an on-line analysis of the background signals acquired at different wavelengths. Third, measurements will be performed at various laser-repetition rates to check for potential recirculation and double-pulsing of the same air mass.

During the MCMA-2006 field campaign, maximum median OH and HO_2 concentra-

tions were measured to be 4.6×10^6 cm^{-3} and 1.9×10^8 cm^{-3}, respectively, during the day. These concentrations are consistent with previous measurements performed in other urban areas, and suggest that OH concentrations are well buffered under highly polluted conditions. In contrast, HO_2 concentrations are observed to be much more sensitive to the level of NO_x due to its fast conversion into OH through reaction with NO, and act as a buffer for OH. A more detailed analysis of these results, including model comparisons, will be presented in a companion paper.

Acknowledgements. The authors are grateful to Xinrong Ren and William Brune for their help during the development of IU-FAGE. The authors also gratefully acknowledge the Molina Center for Energy and the Environment, Gustavo Sosa and the Instituto Mexicano del Petroleo for their help during the MCMA field campaign, and Rafael Ramos of RAMA for the use of one of their NO_x instruments. This research is supported by grants from the National Science Foundation (ATM-9984152 and 0612738) and the Camille and Henry Dreyfus Foundation. Luisa T. Molina would like to acknowledge support from NSF (ATM 0528227).

References

Atkinson, R. and Aschmann, S. M.: OH radical production from the gas-phase reactions of O_3 with a series of alkenes under atmospheric conditions, Environ. Sci. Technol., 27, 1357–1363, 1993.

Bailey, A. E., Heard, D. E., Paul, P. H., and Pilling, M. J.: Collisional quenching of OH($A^2\Sigma^+$,v'=0) by N_2, O_2 and CO_2 between 204 and 294 K. Implications for atmospheric measurements of OH by laser-induced fluorescence, J. Chem. Soc. Faraday T., 93, 2915–2920, 1997.

Clemitshaw, K. C.: A review of instrumentation and measurement techniques for ground-based and airborne field studies of gas-phase tropospheric chemistry, Crit. Rev. Env. Sci. Tec., 34, 1–108, 2004.

Creasey, D. J., Halford-Maw, P. A., Heard, D. E., Pilling, M. J., and Whitaker, B. J.: Implementation and initial deployment of a field instrument for measurement of OH and HO_2 in the troposphere by laser-induced fluorescence, J. Chem. Soc. Faraday T., 93, 2907–2913, 1997.

Creasey, D. J., Halford-Maw, P. A., Heard, D. E., Spence, J. E., and Whitaker, B. J.: Fast photomultiplier tube gating system for photon counting applications, Rev. Sci. Instrum., 69, 4068–4073, 1998.

Dorn, H.-P., Neuroth, R., and Hofzumahaus, A.: Investigation of OH absorption cross sections of rotational transitions in the $A^2\Sigma^+$, v'=0<– $X^2\Pi$, v"=0 band under atmospheric conditions: Implications for tropospheric long-path absorption measurements, J. Geophys. Res., 100, 7397–7409, 1995.

Dubey, M. K., Hanisco, T. F., Wennberg, P. O., and Anderson, J. G.: Monitoring potential photochemical interference in laser-induced fluorescence measurements of atmospheric OH, Geophys. Res. Lett., 23, 3215–3218, 1996.

Dusanter, S., Vimal, D., and Stevens, P. S.: Technical note: Measuring tropospheric OH and HO_2 by laser-induced fluorescence at low pressure – a comparison of calibration techniques, Atmos. Chem. Phys., 8, 321–340, 2008, http://www.atmos-chem-phys.net/8/321/2008/.

Emmerson, K. M., Carslaw, N., Carpenter, L. J., Heard, D. E., Lee, J. D., and Pilling, M. J.: Urban atmospheric chemistry during the PUMA campaign 1: Comparison of modelled OH and HO_2 concentrations with measurements, J. Atmos. Chem., 52, 143–164, 2005a.

Emmerson, K. M., Carslaw, N. and Pilling, M. J.: Urban atmospheric chemistry during the PUMA campaign 2: Radical budgets for OH, HO_2 and RO_2, J. Atmos. Chem., 52, 165–183, 2005b.

Emmerson, K. M., Carslaw, N., Carslaw, D. C., Lee, J. D., McFiggans, G., Bloss, W. J., Gravestock, T., Heard, D. E., Hopkins, J., Ingham, T., Pilling, M. J., Smith, S. C., Jacob, M., and Monks, P. S.: Free radical modelling studies during the UK TORCH campaign in summer 2003, Atmos. Chem. Phys, 7, 167–181, 2007.

Faloona, I. C., Tan, D., Lesher, R. L., Hazen, N. L., Frame, C. L., Simpas, J. B., Harder, H., Martinez, M., Di Carlo, P., Ren, X., and Brune, W. H.: A Laser-Induced Fluorescence Instrument for Detecting Tropospheric OH and HO_2: Characteristics and Calibration, J. Atmos. Chem., 47, 139–167, 2004.

Fenske, J. D., Hasson, A. S., Paulson, S. E., Kuwata, K. T., Ho, A., and Houk, K. N.: The pressure dependence of the OH radical yield from ozone-alkene reactions, J. Phys. Chem. A, 104, 7821–7833, 2000.

George, L. A., Hard, T. M., and OBrien, R. J.: Measurement of free radicals OH and HO_2 in Los Angeles smog, J. Geophys. Res., 104(D9), 11 643–11 645, 1999.

Hard, T. M., George, L. A., and O'Brien, R. J.: An Absolute Calibration for Gas-Phase Hydroxyl Measurements, Environ. Sci. Technol., 36, 1783–1790, 2002.

Heard, D. E. and Pilling, M. J.: Measurement of OH and HO_2 in the troposphere, Chem. Rev., 103, 5163–5198, 2003.

Heard, D. E., Carpenter, L. J., Creasey, D. J., Hopkins, J. R., Lee, J. D., Lewis, A. C., Pilling, M. J., Seakins, P. W., Carslaw, N., and Emmerson, K. M.: High levels of the hydroxyl radical in the winter urban troposphere, Geophys. Res. Lett., 31, L18112, doi:18110.11029/12004GL020554, 2004.

Hofzumahaus, A., Aschmutat, U., Heßling, M., Holland, F., and Ehhalt, D. H.: The measurement of tropospheric OH radicals by laser-induced fluorescence spectroscopy during the POPCORN field campaign, Geophys. Res. Lett., 23, 2541–2544, 1996.

Holland, F., Hessling, M., and Hofzumahaus, A.: In situ measurement of tropospheric OH radicals by laser-induced fluorescence –A description of the KFA instrument, J. Atmos. Sci., 52, 3393–3401, 1995.

Holland, F., A. Hofzumahaus, J. Schafer, A. Kraus, and H. W. Patz: Measurements of OH and HO_2 radical concentrations and photolysis frequencies during BERLIOZ, J. Geophys. Res., 108(D4), 8246, doi:10.1029/2001JD001393, 2003.

Kanaya, Y., Sadanaga, Y., Hirokawa, J., Kajii, Y., and Akimoto, H.: Development of a ground-based LIF instrument for measuring HOx radicals: Instrumentation and calibrations, J. Atmos. Chem., 38, 73–110, 2001.

Kanaya, Y., Cao, R., Akimoto, H., Fukuda, M., Komazaki, Y., Yokouchi, Y., Koike, M., Tanimoto, H., Takegaya, N., and Kondo, Y.: Urban photochemistry in central Tokyo: 1. Observed and modeled OH and HO_2 radical concentrations during the winter and summer 2004, J. Geophys. Res., 112, doi:10.1029/2007JD008670, 2007.

Konrad, S., Schmitz, T., Buers, H.-J., Houben, N., Mannschreck, K., Mihelcic, D., Musgen, P., Patz, H.-W., Holland, F., Hofzumahaus, A., Schafer, H.-J., Schroder, S., and Volz-Thomas, A.: Hydrocarbon measurements at Pabstthum during the BERLIOZ campaign and modeling of free radicals, J. Geophys. Res., 108(D4), 8251, doi:10.1029/2001JD000866, 2003.

Kroll, J. H., Clarke, J. S., Donahue, N. M., Anderson, J. G., and Demerjian, K. L.: Mechanism of HO_x formation in the gas-phase ozone-alkene reaction. 1. Direct pressure-dependent measurements of prompt OH yields, J. Phys. Chem. A, 105, 1554–1560, 2001a.

Kroll, J. H., Sahay, S. R., Anderson, J. G., Demerjian, K. L., and Donahue, N. M.: Mechanism of HO_x formation in the gas-phase ozone-alkene reaction. 2. Prompt versus thermal

dissociation of carbonyl oxides to form OH, J. Phys. Chem. A, 105, 4446–4457, 2001b.
Levy, H.: Normal atmosphere: large radical and formadehyde concentrations predicted, Science, 173, 141–143, 1971.
Levy, H.: Photochemistry of the lower troposhere, Planet. Space Sci., 20, 919–935, 1972.
Martinez, M., Harder, H., Kovacs, T. A., Simpas, J. B., Bassis, J., Lesher, R., Brune, W. H., Frost, G. J., Williams, E. J., Stroud, C. A., Jobson, B. T., Roberts, J. M., Hall, S. R., Shetter, R. E., Wert, B., Fried, A., Alicke, B., Stutz, J., Young, V. L., White, A. B., and Zamora, R. J.: OH and HO_2 concentrations, sources, and loss rates during the Southern Oxidants Study in Nashville, Tennessee, summer 1999, J. Geophys. Res., 108(D19), 4617, doi:10.1029/2003JD003551, 2003
Martinez, M., Harder, H., Ren, X., Lesher, R. L., and Brune, W. H.: Measuring atmospheric naphtalene with laser-induced fluorescence, Atmos. Chem. Phys, 4, 563–569, 2004.
Mather, J. H., Stevens, P. S., and Brune, W. H.: OH and HO_2 measurements using laser-induced fluorescence, J. Geophys. Res., 102, 6427–6436, 1997.
Molina, L. T. and Molina, M. J.: Air Quality in the Mexico Megacity: An Integrated Assessment, Kluwer Academic Publishers: Dordrecht, The Netherlands, 384 pp., 2002.
Molina, L. T., Kolb, C. E., de Foy, B., Lamb, B. K., Brune, W. H., Jimenez, J. L., Ramos-Villegas, R., Sarmiento, J., Paramo-Figueroa, V. H., Cardenas, B., Gutierrez-Avedoy, V., and Molina, M. J.: Air quality in North America's most populous city - overview of the MCMA-2003 campaign, Atmos. Chem. Phys., 7, 2447–2473, 2007, http://www.atmos-chem-phys.net/7/2447/2007/.
Molina, M. J. and Molina, L. T.: Megacities and atmospheric pollution, J. Air Waste Manage., 54, 644–680, 2004.
Paulson, S. E. and Orlando, J. J.: The reactions of ozone with alkenes: An important source of HO_x in the boundary layer, Geophys. Res. Lett., 23, 3727–3730, 1996.
Platt, U., Alicke, B., Dubois, R., Geyer, A., Hofzumahaus, A., Holland, F., Martinez, M., Mihelcic, D., Klupfel, T., Lohrmann, B., Patz, W., Perner, D., Rohrer, F., Schafer, J., and Stutz, J.: Free radicals and fast photochemistry during BERLIOZ, J. Atmos. Chem., 42, 359–394, 2002.
Raga, G. B. and Raga, A. C.: On the formation of an elevated ozone peak in Mexico City, Atmos. Environ., 34, 4097–4102, 2000.
Ren, X., Harder, H., Martinez, M., Lesher, R. L., Oliger, A., Shirley, T., Adams, J., Simpas, J. B., and Brune, W. H.: HO_x concentrations and OH reactivity observations in New York City during PMTACS-NY2001, Atmos. Environ., 37, 3627–3637, 2003a.

Ren, X., Harder, H., Martinez, M., Lesher, R. L., Oliger, A., Simpas, J. B., Brune, W. H., Schwab, J. J., Demerjian, K. L., He, Y., Zhou, X., and Gao, H.: OH and HO_2 Chemistry in the urban atmosphere of New York City, Atmos. Environ., 37, 3639–3651, 2003b.

Ren, X., Harder, H., Martinez, M., Faloona, I. C., Tan, D., Lesher, R. L., Di Carlo, P., Simpas, J. B., and Brune, W. H.: Interference Testing for Atmospheric HO_x Measurements by Laser-induced Fluorescence, J. Atmos. Chem., 47, 169–190, 2004.

Ren, X., Brune, W. H., Mao, J., Mitchell, M. J., Lesher, R. L., Simpas, J. B., Metcalf, A. R., Schwab, J. J., Cai, C., Li, Y., Demerjian, K. L., Felton, H. D., Boynton, G., Adams, A., Perry, J., He, Y., Zhou, X., and Hou, J.: Behavior of OH and HO_2 in the winter atmosphere in New York City, Atmos. Environ., 40, S252–S253, 2006.

Shirley, T. R., Brune, W. H., Ren, X., Mao, J., Lesher, R., Cardenas, B., Volkamer, R., Molina, L. T., Molina, L. T., Lamb, B., Velasco, E., Jobson, T., and Alexander, M.: Atmospheric oxidation in the Mexico City Metropolitan Area (MCMA) during April 2003, Atmos. Chem. Phys., 6, 2753–2765, 2006, http://www.atmos-chem-phys.net/6/2753/2006/.

Stevens, P. S., Mather, J. H., and Brune, W. H.: Measurements of tropospheric OH and HO_2 by laser-induced fluorescence at low pressure, J. Geophys. Res., 99, 3543–3557, 1994.

Volkamer, R., Sheehy, P. M., Molina, L. T., and Molina, M. J.: Oxidative capacity of the Mexico City atmosphere – Part 1: A radical source perspective, Atmos. Chem. Phys. Discuss., 7, 5365–5412, 2007, http://www.atmos-chem-phys-discuss.net/7/5365/2007/.

Wennberg, P. O., Hanisco, T. F., Cohen, R. C., Stimpfle, R. M., Lapson, L. B., and Anderson, J. G.: In situ measurements of OH and HO_2 in the upper troposphere and stratosphere, J. Atmos. Sci., 52, 3413–3420, 1995.

Table 1. Chronologic compilation of the urban and suburban field campaigns that include HO_x measurements. The numbers in brackets are median values. [a] $P(O_3)$ calculated from measured HO_2 and RO_2 concentrations. [b] $P(O_3)$ calculated from measured HO_2 concentrations. [c] Range of HO_2/OH ratios from binned NO. $P(O_3)$ is the value at the peak. [d] $P(O_3)$ calculated from a box model that took into account all the reactions converting NO into NO_2. [e] The contribution of HONO was calculated after subtraction of the OH+NO sink.

Field Campaigns	Measured OH(10^6 cm^{-3})	Measured HO_2(10^8 cm^{-3})	Measured O_3, NO, NO_2(ppb)	HO_2/OH	$P(O_3)$ (ppb/h)	Daytime model comparison Calculated/Measured	RO_x Sources	References
LAFRE, Free Radical Experiment Claremont, Los Angeles (CA), September 1993	4.0–6.0	1.6–2.0	Peak O_3:140-200 NO_x:20-90			Lumped mechanism: CAL, OH:1.5 at midday, HO_2:>1 at midday	HONO, O_3, HCHO, dialdehyde, O_3-alkene	George et al. (1999)
BERLIOZ, Berliner Ozonexperiment Pabstthum, Berlin, July–August 1998	2.0–8.0 (3.5)	0.5–8.5 (2.2)	O_3: – NO:<0.1–1.5 NO_2:1.5–5.5	0–200	(8)[a]	OH:NO_x>5 ppb: good for MCM and RACM NO_x<5 ppb: 1.25 at midday (MCM), 2(RACM) HO_2:good (MCM), 1.4 (RACM)	O_3, HCHO, HONO, O_3-alkene	Platt et al. (2002) Holland et al. (2003) Konrad et al. (2003)
PUMA, Pollution of the Urban Midlands Atmosphere Birmingham (UK), June–July 1999	2.0–9.0	1.5–10.0	O_3:29.0–41.2 NO:2.7–4.2 NO_2:6.6–14.4	20–160		MCM 3.1, OH:0.58, HO_2:0.56 HONO, O_3	OVOCs, O_3-alkene, HCHO,	Heard et al. (2004) Emmerson et al. (2005a) Emmerson et al. (2005b)
SOS, Southern Oxidants Study, Nashville (TN) June–July 1999	7.0–20(10.0)	2.8–22.4 (7.5)	O_3:<1–90 NO:0.1–70 NO_2: –		(14.5)[b]	Lumped mechanism, OH:0.75, HO_2:0.64	O_3, HCHO, HONO	Martinez et al. (2003)
PUMA, Pollution of the Urban Midlands Atmosphere Birmingham (UK), January–February 2000	0.5–4.0	1.5–10.0	O_3:13.2–22.0 NO:4.5–20.5 NO_2:9.3–22.9			MCM 3.1, OH:0.50, HO_2:0.49	O_3-alkene, OVOCs, HONO	Heard et al. (2004) Emmerson et al. (2005a Emmerson et al. (2005b)
PMTACS-NY, PM2.5 Technology Assessment and Characterization Study- -New York, June–August 2001	5.0–20.0(7.0)	0.5–6.0(1.0)	Peak O_3: (48) NO_x: (20–48)	(5–70)[c]	(20)[b]	RACM, OH:0.91, HO_2:0.81, agreement better at low NO_x	HONO, O_3-alkene	Ren et al. (2003a) Ren et al. (2003b)
MCMA-2003, Mexico City Metropolitan Area Mexico City, April 2003	5.0–8.0 (7.0)	3.0–12.0(7.4)	Peak O_3: (115) Peak NO_x: (86)	8–250 (20–150)[c]	(48)[b]	RACM (morning-midday), OH:0.93-1.30, HO_2:0.86-1.27		Shirley et al. (2006) Volkamer et al. (2007)
TORCH, Tropospheric Organic Chemistry experiment London, England, July–August 2003	1.2–7.5	0.2–3.3	Average O_3:20.8–95.2 Average NO:0.3–9.9 Average NO_2:1.5–13.2	2–500 (10–70)[c]	(7.2)[d]	MCM 3.1, OH:1.24, HO_2:1.07	OVOCs, O_3-alkene, O_3, HONO, HCHO	Emmerson et al. (2007)
PMTACS-NY, PM2.5 Technology Assessment and Characterization Study- -New York, January–February 2004	(1.4)	(0.2)	Peak O_3:(20) NO:(7–30) NO_2: (15–30)	50–400		RACM, Median OH:1.02, Median HO_2:0.17	HONO, [e]O_3-alkene	Ren et al. (2006)
IMPACT IV, Integrated Measurements Program for Aerosol and oxidant Chemistry in Tokyo,Japan, January–February 2004	(1.5)	(1.1 ppt)	Peak O_3: (30) NO:1–70 (8.1) NO_2: (18.2)	1–80 (3–30)[c]		RACM,OH:0.93–1.23, HO_2:0.48–0.88	O_3-alkene, OVOCs, HONO[e]	Kanaya et al. (2007)
IMPACT L, Integrated Measurements Program for Aerosol and oxidant Chemistry in Tokyo, Japan,July–August 2004	(6.3)	(5.7 ppt)	Peak O_3: (30) NO:0.1–20 (2.6) NO_2: (9.4)	1–700 (5–400)[c]		RACM,OH:0.86, HO_2:1.29	OVOCs, O_3, O_3-alkene, HONO[e]	Kanaya et al. (2007)
MCMA-2006, Mexico City Metropolitan Area Mexico City, March 2006	2.0–15.0 (4.6)	0.6–4.5 (1.9)	Peak O_3: (90) Peak NO: (200) Peak NO_2: (80)	1–300 (8–70)[c]	(80)[b]	S. Dusanter et al.: Measurements of OH and HO_x Concentrations During the MCMA-2006 Field Campaign: Part 2-Model Comparison and Radical Budget,in preparation		This work

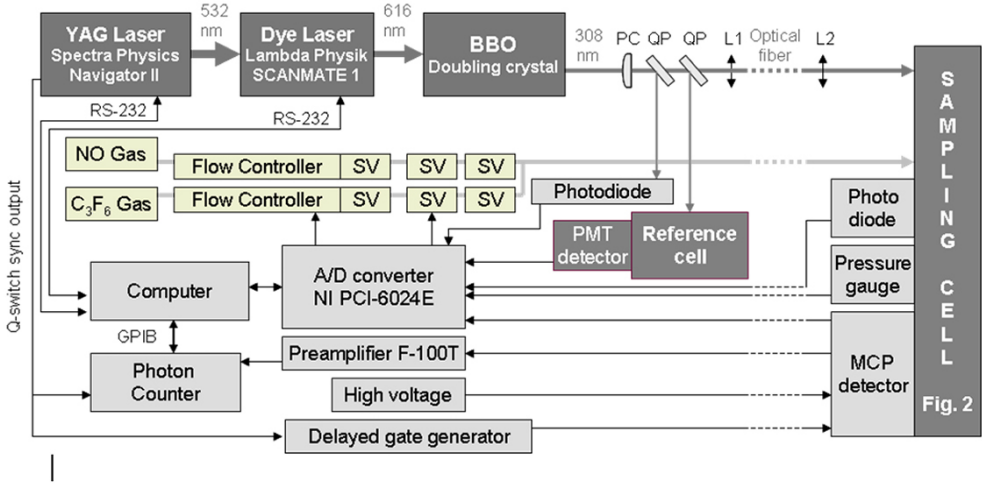

Fig. 1. Schematic diagram of the IU-FAGE instrument. PC: planoconvex lens, QP: quartz plate, L1 and L2: optical launchers, SV: solenoid valve, MCP: microchannel plate.

ACPD
8, 13689–13739, 2008

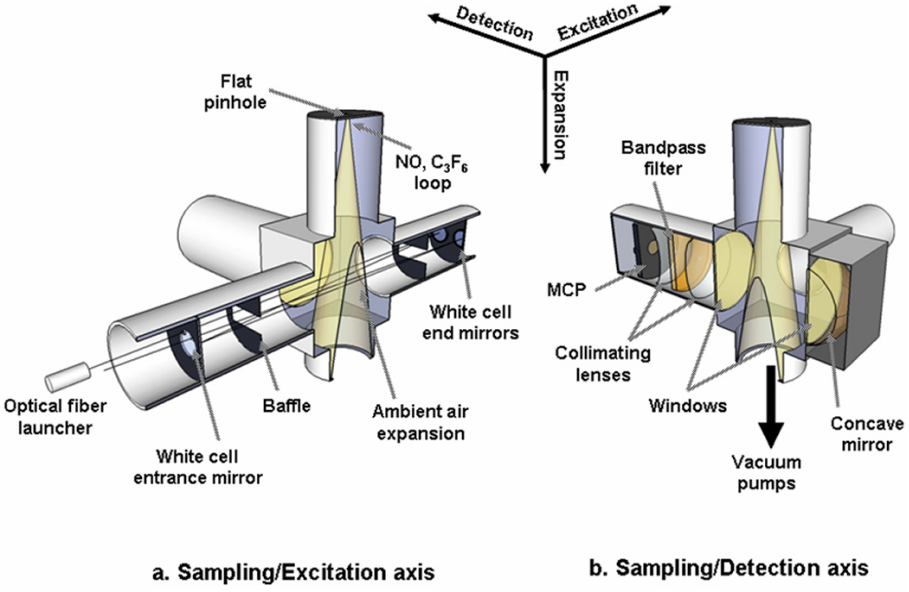

Fig. 2. Cross-sections of the detection cell. The left figure displays the intersection between the sampled air mass and the excitation beam through the multipass cell. The right figure displays the detection axis.

ACPD
8, 13689–13739, 2008

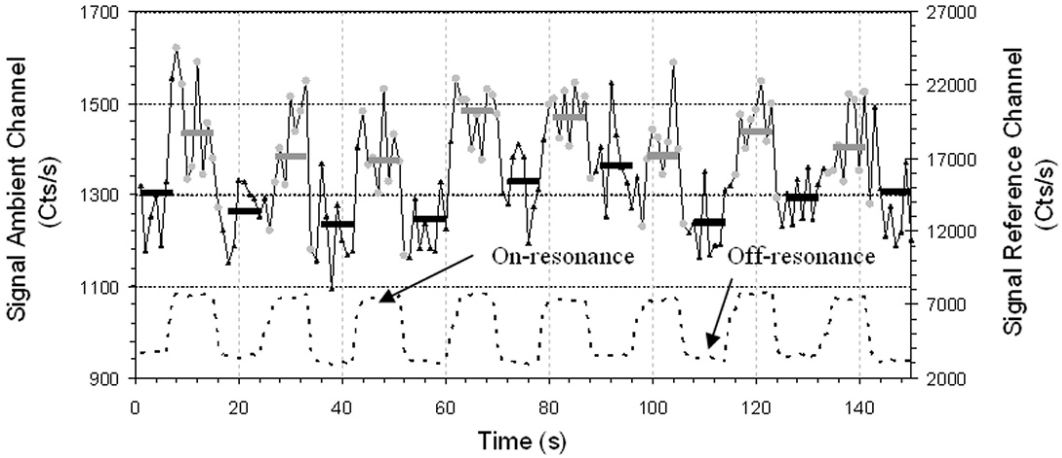

Fig. 3. Segment of raw data recorded on 15 March with a 10 s modulation cycle. The solid black line corresponds to the signal recorded from the ambient channel. The grey circles and the grey symbols are the 1 s on-resonance signal and the averaged 10 s signal, respectively. The black triangles and the black symbols are the 1 s background signal and the 10 s averaged background signal. The dashed black line corresponds to the signal recorded from the reference channel and indicates when the measurements are performed on- and off-resonance.

ACPD
8, 13689–13739, 2008

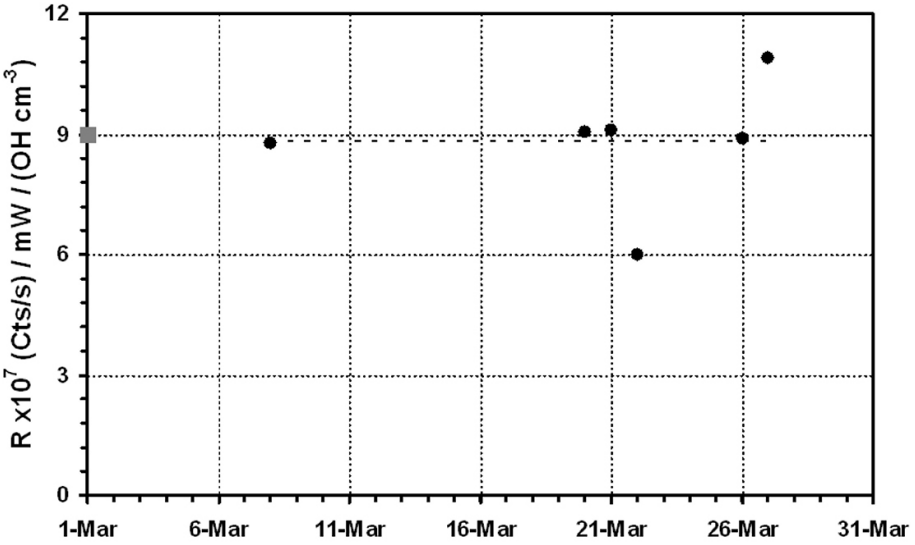

Fig. 4. The black circles represent the calibration performed during the MCMA-2006 field campaign using the O_3-alkene calibration technique described in Dusanter et al. (2008). The grey square plotted on 1 March represents the average value for calibrations performed during laboratory tests prior to MCMA-2006.

ACPD
8, 13689–13739, 2008

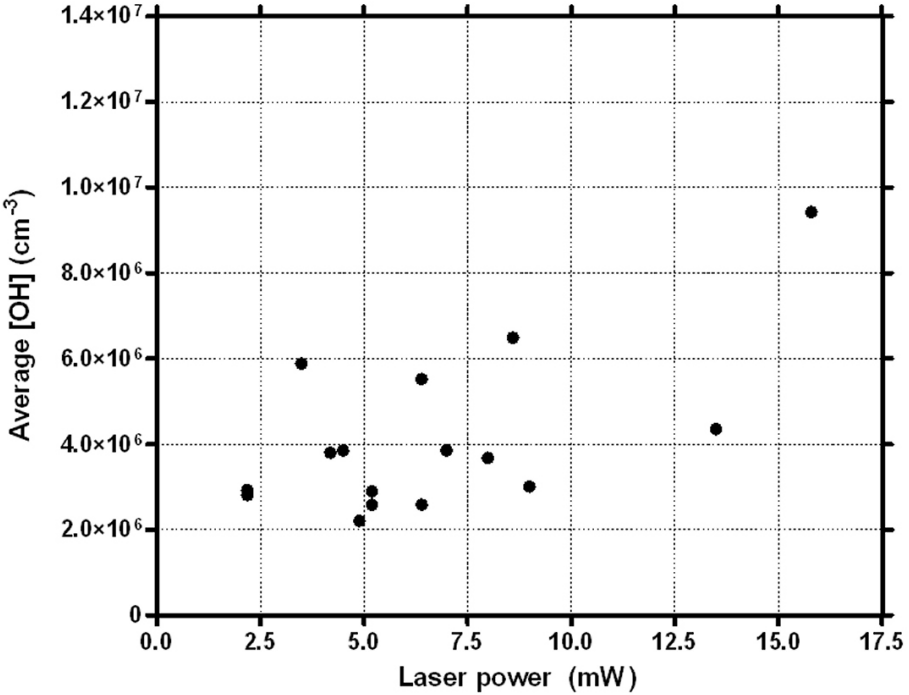

Fig. 5. Average OH concentrations (10 a.m. to 5 p.m.) measured between 14 and 31 March as a function of the average laser power.

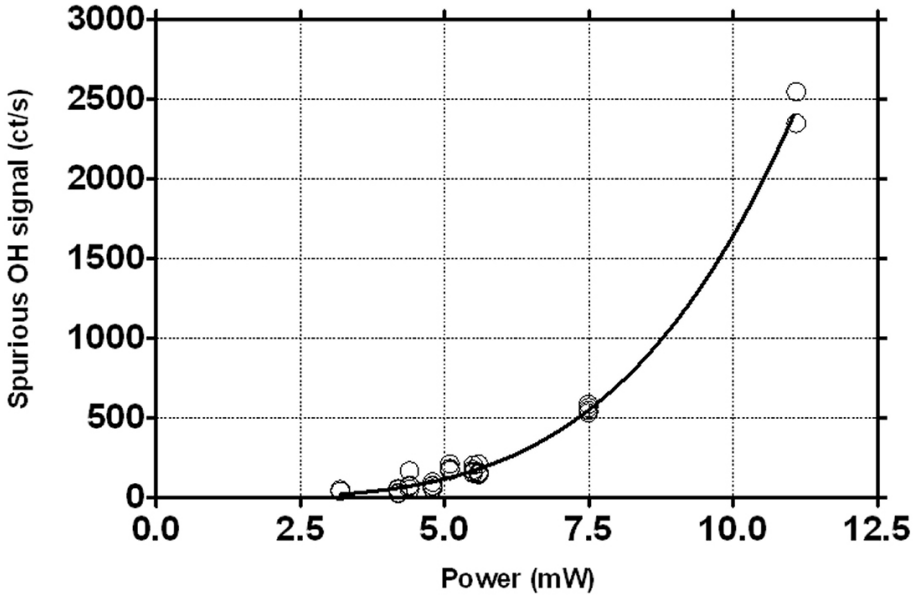

Fig. 6. Calibration of the spurious OH produced during HO_2 measurements in clean air. S_{OH} was measured at various laser power and various NO flows during the MCMA-2006 field campaign. S_{OH} was found to be linear with NO and was therefore normalized to 1 SCCM of NO. The circles display all the measurements performed on nine different days during the campaign. The black line is a non-linear fit of the measurements using a power function.

ACPD

8, 13689–13739, 2008

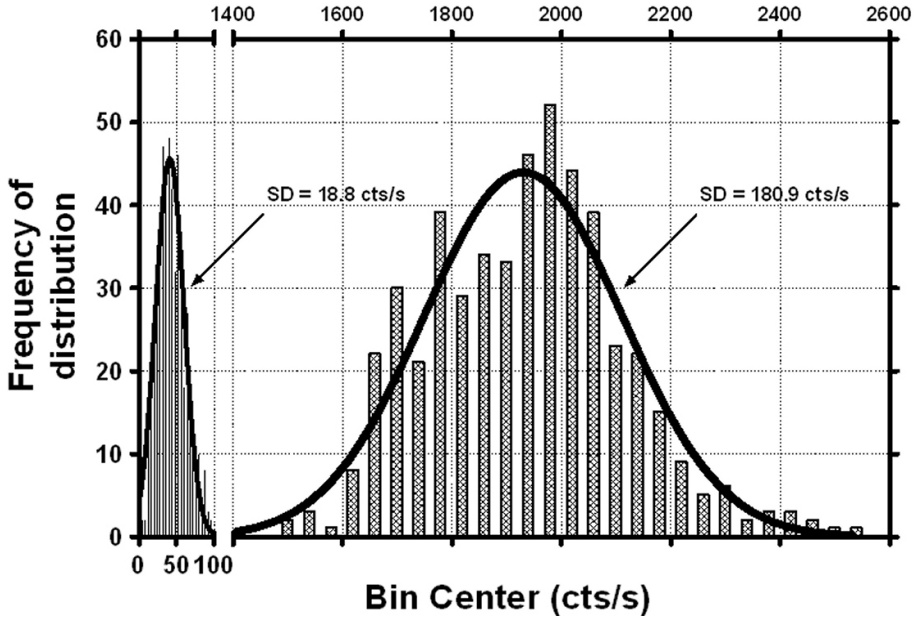

Fig. 7. Distribution of the background signal. The left portion of the figure represent the distribution of the background signal (537 points, bin width of 4 cts/s) observed during calibration experiment performed at a laser power of 3.6 mW. The right portion displays a similar distribution (502 points, bin width of 40 cts/s) observed on 27 March during the MCMA-2006 at a laser power of 4.0 mW.

ACPD
8, 13689–13739, 2008

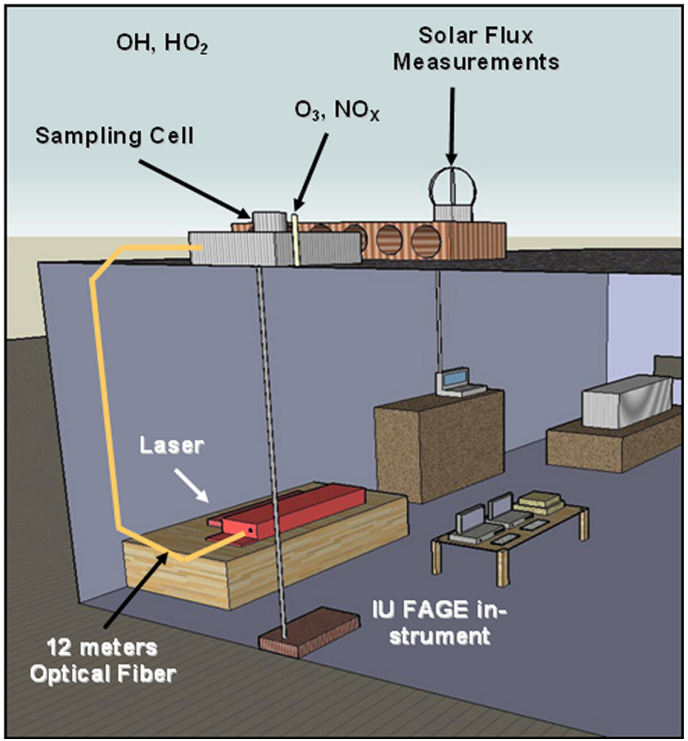

Fig. 8. Configuration of the IU-FAGE instrument during the MCMA 2006 field campaign.

ACPD
8, 13689–13739, 2008

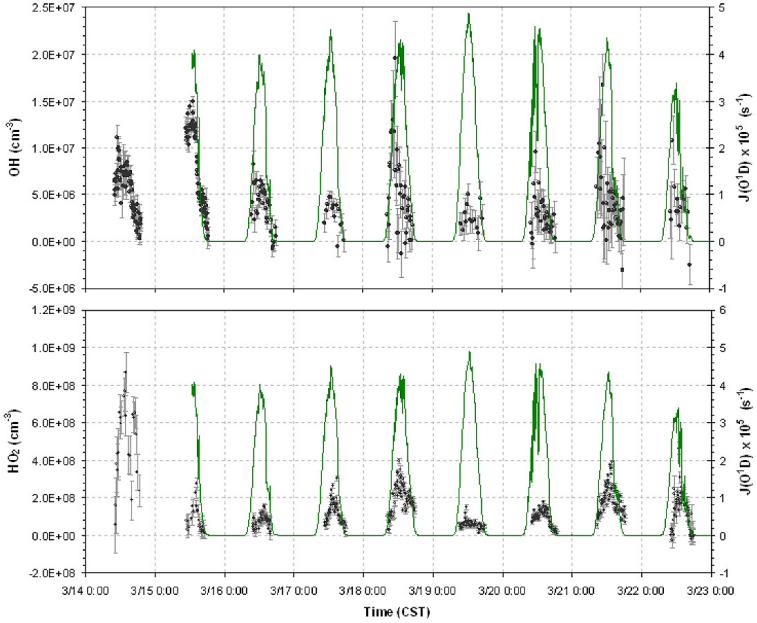

Fig. 9. OH and HO_2 diurnal profiles from 14 to 22 March. The upper panel displays the measured OH concentrations using black circles. The OH measurements are averaged for 7.5 min for 14 and 15 March, 15 min for 16 March, and 30 min for 17–22 March). The lower panel displays the measured HO_2 concentrations using black circles and an integration time of 15 s. For both panels, the green line corresponds to the measured $J(O^1D)$ values and error bars are the precision (1σ) on the HO_x measurements.

ACPD
8, 13689–13739, 2008

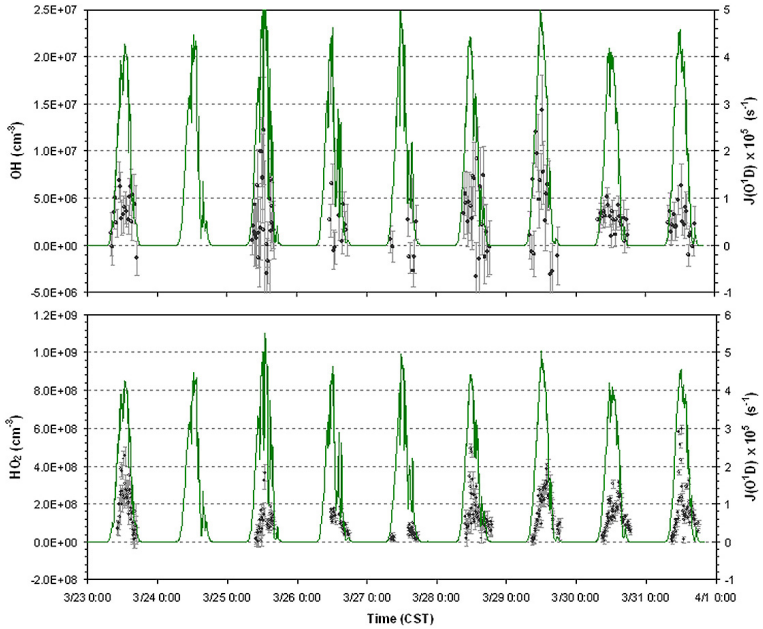

Fig. 10. OH and HO_2 diurnal profiles from 23 to 31 March. The upper panel displays the measured OH concentrations using black circles with an integration time of 30 min. The lower panel displays the measured HO_2 concentrations using black circles and an integration time of 15 s. For both panels, the green line corresponds to the measured $J(O^1D)$ values and error bars are the precision (1σ) on the HO_x measurements.

ACPD
8, 13689–13739, 2008

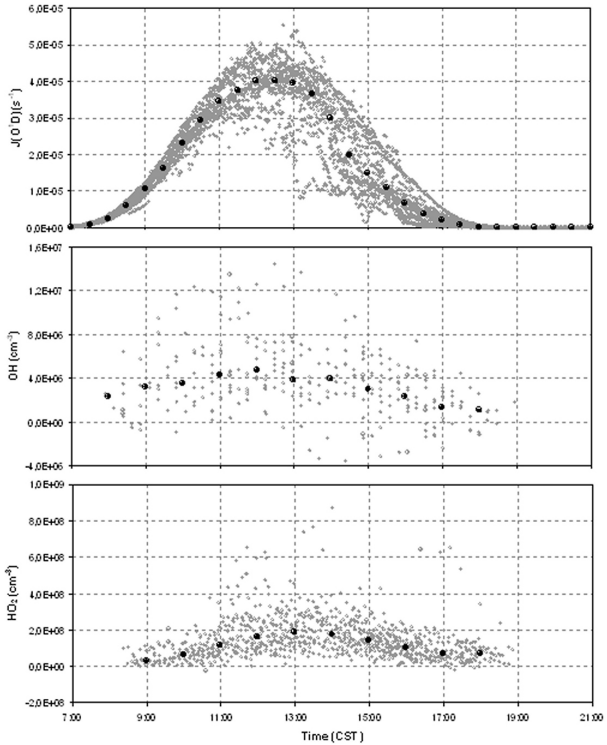

Fig. 11. Median J(O^1D), OH and HO_2. Grey symbols are individual measurements and black symbols are the medians calculated on data binned with a time interval of 10 min for J(O^1D) and 30 min for OH and HO_2. OH concentrations displayed on the middle panel were averaged for 30 min for each individual day. HO_2 concentrations displayed on the lower panel are individual measurements averaged for 15 s for each individual day.

ACPD
8, 13689–13739, 2008

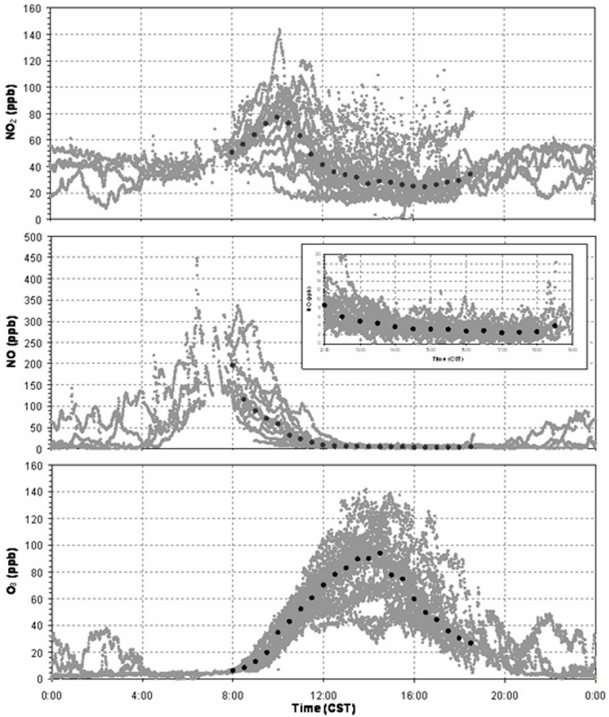

Fig. 12. Median NO, NO_2 and O_3. Grey symbols are individual measurements averaged for 1 min and black symbols are the medians calculated on data binned with a time interval of 10 min. Daytime data between 8 a.m. and 6 p.m. were recorded from 14–31 March. The remaining data was recorded between 26–31 March.

ACPD
8, 13689–13739, 2008

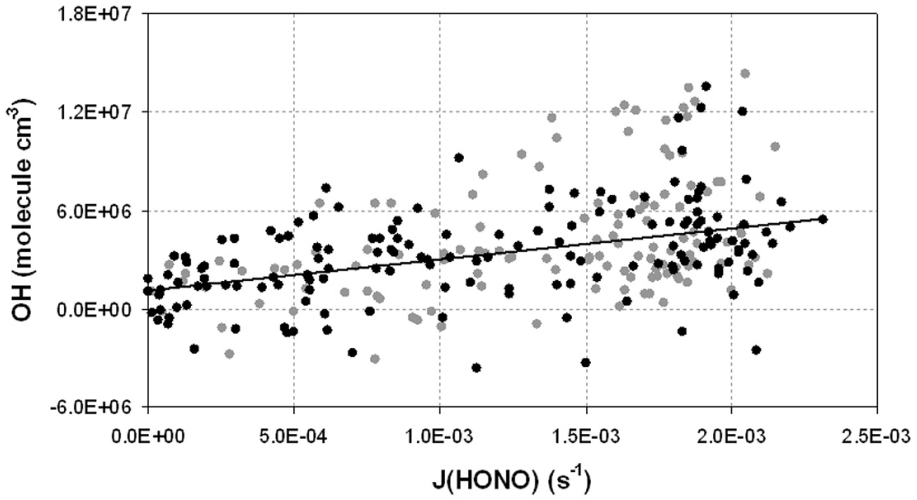

Fig. 13. Correlation plots between HO_x radicals and J(HONO). Daily measurements are averaged for 30 min over the whole campaign. The grey circles display measurements performed under high NO_x conditions before noon (3.4<NO<292 ppb, 15.8<NO_2<127.1 ppb). Black circles display measurements performed under lower NO_x conditions (0.2<NO<13.5 ppb, 0.7<NO_2<77.1).

ACPD
8, 13689–13739, 2008

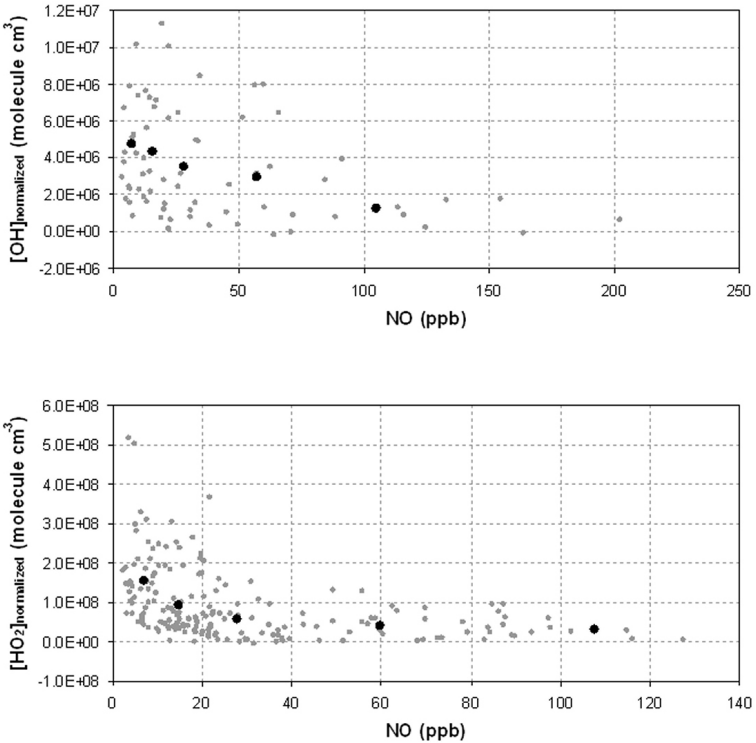

Fig. 14. Correlation plot between normalized HO_x concentrations and NO. 30 min median of daily OH and HO_2 concentrations are normalized to J(HONO) (see text). Grey circles display the measurements performed before noon. Black circles are medians based on binned NO.

ACPD
8, 13689–13739, 2008

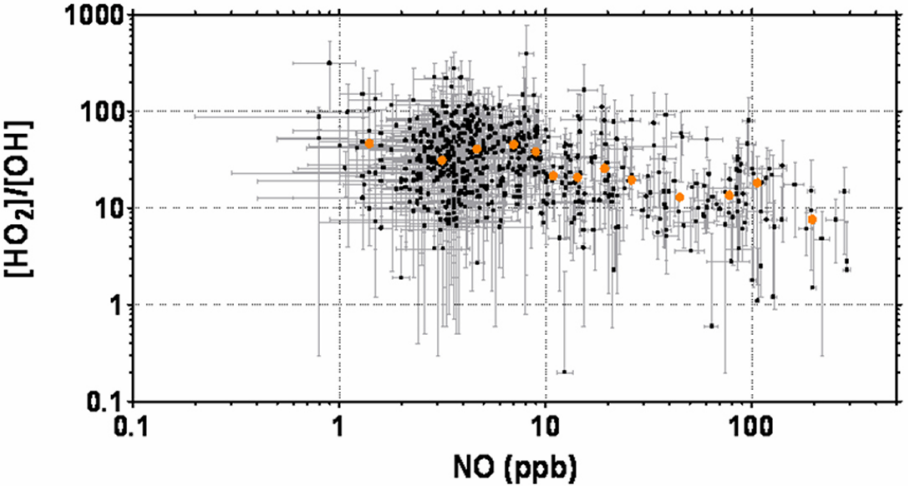

Fig. 15. Correlation plot between HO_2/OH ratio and NO. Black symbols are individual measurements and orange symbols are the median calculated on binned NO data.

ACPD
8, 13689–13739, 2008

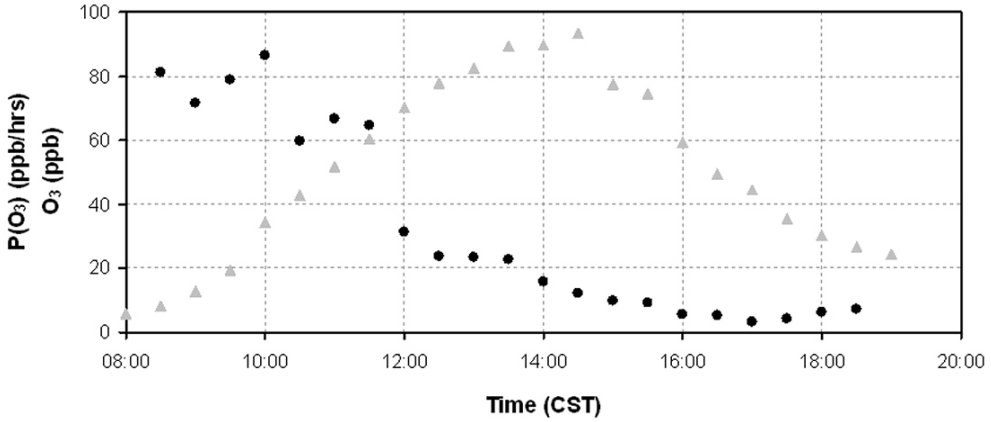

Fig. 16. Median instantaneous O_3 production by HO_x radicals (black circles) and median ozone measurements (grey circles) from 14 to 31 March.

ACPD
8, 13689–13739, 2008